12 SCIENTIFIC HIGHLIGHT OF THE MONTH

An Introduction to Maximally-Localized Wannier Functions

Nicola Marzari[1], Ivo Souza[2], and David Vanderbilt[2]

[1] *Department of Materials Science and Engineering, Massachusetts Institute of Technology, Cambridge, MA 02139-8407*

[2] *Department of Physics and Astronomy, Rutgers University, Piscataway, NJ 08854-8019*

Abstract

The electronic ground state of a periodic system is usually described in terms of extended Bloch orbitals, simultaneous eigenstates of the periodic Hamiltonian and of the direct lattice translations. An alternative representation in terms of localized orbitals has been introduced by Gregory Wannier in 1937; besides its theoretical relevance in several areas of solid-state theory, it has gained recent prominence due to its connection with the Berry-phase theory of bulk polarization, the interest in linear-scaling approaches, and with the development of general algorithms to derive Wannier functions in the framework of first-principles electronic structure calculations. The connection between the Bloch representation and the Wannier representation is realized by families of transformations in a continuous space of unitary matrices, carrying a large degree of arbitrariness. A few years ago we have developed a localization algorithm that allows one to iteratively transform the extended Bloch orbitals of a first-principles calculation into a unique set of *maximally-localized* Wannier functions (MLWFs), extending and encompassing Boys formulation for molecules to the solid-state case. The localization algorithm is independent of the single-particle electronic structure approach adopted, or the choice of basis set, and it is straightforwardly applied to extended or periodic solids and to isolated systems. Additionally, a novel disentanglement procedure allows to extract a maximally-connected manifold of any chosen dimension from a given energy window, leading to the extension of the original algorithm to the case of systems without gaps (e.g., metals) and removing the limitation to isolated groups of bands separated by gaps from higher and lower manifolds. In this Highlight we will outline and summarize the main results of the theory and algorithm underlying the maximally-localized Wannier-functions representation, and review some of the applications that have since appeared in the literature.

1 Introduction

The electronic ground state of a periodic solid, in the independent-particle approximation, is naturally labeled according to the prescriptions of Bloch's theorem: single-particle orbitals are assigned a quantum number $\mathbf{k}$ for the crystal momentum, together with a band index n. Although this choice is widely used in electronic structure calculations, alternative representations are available. The Wannier representation [1, 2, 3], essentially a real-space picture of localized orbitals, assigns as quantum numbers the lattice vector $\mathbf{R}$ of the cell where the orbital is localized, together with a band-like index n.

Wannier functions can be a powerful tool in the study of the electronic and dielectric properties of materials: they are the solid-state equivalent of "localized molecular orbitals" [4, 5, 6, 7], and thus provide an insightful picture of the nature of chemical bonding, otherwise missing from the Bloch picture of extended orbitals. By transforming the occupied electronic manifold into a set of maximally-localized Wannier functions (MLWFs), it becomes possible to obtain an enhanced understanding of chemical coordination and bonding properties via an analysis of factors such as changes in shape or symmetry of the MLWFs, or changes in the locations of their centers of charge. In particular, the charge center of a MLWF provides a kind of classical correspondence for the "location of an electron" (or electron pair) in a quantum-mechanical insulator, allowing for the definition of insightful pair-distribution functions between electrons and ions. This analogy is extended further by the modern theory of bulk polarization [8, 9], which directly relates the vector sum of the centers of the Wannier functions to the macroscopic polarization of a crystalline insulator. Thus, the heuristic identification by which the displacements of the Wannier centers provide a microscopic map of the local polarization field is augmented, via the theory of polarization, by an exact statement relating the sum of displacements to the exact quantum-mechanical polarization of the system. Beside the above points, which are of obvious physical and chemical interest, the MLWFs are now also being used as a very accurate minimal basis for a variety of algorithmic or theoretical developments, with recent applications ranging from linear-scaling approaches [10] to the construction of effective Hamiltonians for the study of ballistic transport [11], strongly-correlated electrons [12, 13, 14], self-interaction corrections, and photonic lattices [15, 16].

Wannier functions are strongly non-unique. This is a consequence of the phase indeterminacy $e^{i\phi_n(\mathbf{k})}$ that Bloch orbitals $\psi_{n\mathbf{k}}$ have at every wavevector $\mathbf{k}$. This indeterminacy is actually more general than just the phase factors; Bloch orbitals belonging to an isolated group of bands (i.e., a set of bands that are connected between themselves by degeneracies, but separated from others by energy gaps) can undergo arbitrary unitary transformations $U^{(\mathbf{k})}$ between themselves at every $\mathbf{k}$. We have recently developed a procedure [17] that can iteratively refine these otherwise arbitrary degrees of freedom, so that they lead to Wannier functions that are well defined and that are localized around their centers (in particular, they minimize the second moment around the centers). Such a procedure can be applied either to an entire band complex of Bloch orbitals, or just to some isolated subgroups.

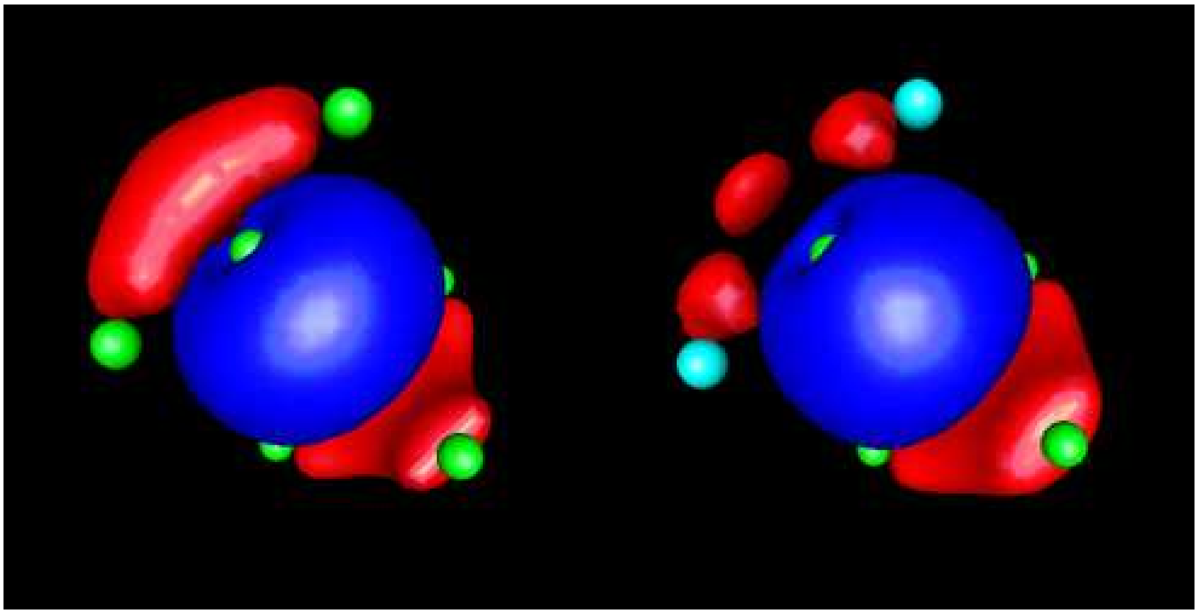

Figure 1: Amplitude isosurface contours for maximally-localized Wannier functions in Si (left panel) and GaAs (right panel). Red and blue contours are for isosurfaces of identical absolute value but opposite signs; Si and As atoms are in green, Ga in cyan. Each unit cell displays four (spin-unpolarized) equivalent WFs, localized around the centers of the four covalent bonds; breaking of inversion symmetry in GaAs polarizes the WFs towards the more electronegative As anion.

2 Method

Electronic structure calculations are often carried out using periodic boundary conditions. This is the most natural choice for the study of perfect crystals and for minimizing finite-size effects in the study of several non-periodic systems (e.g., surfaces or impurities). The one-particle effective Hamiltonian $\hat{H}$ then commutes with the lattice-translation operator $\hat{T}_{\mathbf{R}}$, allowing one to choose as common eigenstates the Bloch orbitals $|\,\psi_{n\mathbf{k}}\,\rangle$,

$$[\,\hat{H},\,\hat{T}_{\mathbf{R}}\,] \;=\; 0 \;\;\Rightarrow\;\; \psi_{n\mathbf{k}}(\mathbf{r}) \;=\; e^{i\phi_n(\mathbf{k})}\,u_{n\mathbf{k}}(\mathbf{r})\,e^{i\mathbf{k}\cdot\mathbf{r}} \;\;, \tag{1}$$

where $u_{n\mathbf{k}}(\mathbf{r})$ has the periodicity of the Hamiltonian. There is an arbitrary phase $\phi_n(\mathbf{k})$, periodic in reciprocal space, that is not assigned by the Schrödinger equation and that we have written out explicitly. We obtain a (non-unique) Wannier representation using any unitary transformation of the form $\langle\, n\mathbf{k}\,|\,\mathbf{R}n\,\rangle = e^{i\varphi_n(\mathbf{k})\,-i\mathbf{k}\cdot\mathbf{R}}$:

$$|\,\mathbf{R}n\,\rangle \;=\; \frac{V}{(2\pi)^3}\int_{BZ}|\,\psi_{n\mathbf{k}}\,\rangle\, e^{i\varphi_n(\mathbf{k})\,-i\mathbf{k}\cdot\mathbf{R}}\,d\mathbf{k} \;\;. \tag{2}$$

Here V is the real-space primitive cell volume, and $\varphi_n(\mathbf{k}+\mathbf{G}) = \varphi_n(\mathbf{k})$, for any reciprocal-lattice translation $\mathbf{G}$. It is easily shown that the $|\,\mathbf{R}n\,\rangle$ form an orthonormal set, and that two Wannier functions $|\,\mathbf{R}n\,\rangle$ and $|\,\mathbf{R}'n\,\rangle$ transform into each other with a translation of a lattice vector $\mathbf{R}-\mathbf{R}'$ [18]. The arbitrariness that is present in $\varphi_n(\mathbf{k})$ [or $\phi_n(\mathbf{k})$] propagates to the resulting Wannier functions, making the Wannier representation non-unique.

Since the electronic energy functional in an insulator is also invariant with respect to a unitary transformation of its N occupied Bloch orbitals, there is additional freedom associated with the choice of a full unitary matrix (and not just a diagonal one) transforming the orbitals between themselves at every wavevector $\mathbf{k}$. Thus, the most general operation that transforms the Bloch orbitals into Wannier functions is given by

$$| \mathbf{R}n \rangle \;=\; \frac{V}{(2\pi)^3} \int_{BZ} \sum_{m=1}^{N} U_{mn}^{(\mathbf{k})} \, | \psi_{m\mathbf{k}} \rangle \, e^{-i\mathbf{k}\cdot\mathbf{R}} \, d\mathbf{k} \;\;, \tag{3}$$

where $U_{mn}^{(\mathbf{k})}$ is a unitary matrix of dimension N. Alternatively, we can regard this as a two-step process in which one first constructs Bloch-like orbitals

$$| \widetilde{\psi}_{n\mathbf{k}} \rangle = \sum_{m=1}^{N} U_{mn}^{(\mathbf{k})} \, | \psi_{m\mathbf{k}} \rangle \tag{4}$$

and then constructs Wannier function $| w_n \rangle$ from the manifold of states $| \widetilde{\psi}_{n\mathbf{k}} \rangle$. The extra unitary mixing may be optional in the case of a set of discrete bands that do not touch anywhere in the Brillouin zone, but it is mandatory when describing a case like that of the four occupied bands of silicon, where there are degeneracies at symmetry points in the Brillouin zone. An attempt to construct a single Wannier function from the single lowest-energy or highest-energy band would be doomed in this case, because of non-analyticity of the Bloch functions in the neighborhood of the degeneracy points. Instead, the introduction of the unitary matrices $U_{mn}^{(\mathbf{k})}$ allows for the construction of states $| \widetilde{\psi}_{n\mathbf{k}} \rangle$ that are everywhere smooth functions of $\mathbf{k}$. In this case, the Wannier functions $w_n(\mathbf{r}-\mathbf{R}) = | \mathbf{R}n \rangle$, can be shown to be well localized: for a $\mathbf{R}_i$ far away from $\mathbf{R}$, $w_n(\mathbf{R}_i - \mathbf{R})$ is a combination of terms like $\int_{BZ} \; u_{m\mathbf{k}}(0) e^{i\mathbf{k}\cdot(\mathbf{R}_i-\mathbf{R})} \, d\mathbf{k}$, which are small due to the rapidly varying character of the exponential factor [18]. By way of illustration, the MLWFs that result from our procedure for the cases of Si and GaAs are shown in Fig. 1.

2.1 Maximally-localized Wannier functions

Several heuristic approaches have been developed that construct reasonable sets of Wannier functions, reducing the arbitrariness in the $U_{mn}^{(\mathbf{k})}$ with symmetry considerations and analyticity requirements [20, 21], or explicitly employing projection techniques on the occupied subspace spanned by the Bloch orbitals [22, 23] At variance with those approaches, we introduce a well-defined *localization criterion*, choosing the functional

$$\Omega = \sum_n \left[\langle \mathbf{0}n \,|\, r^2 \,|\, \mathbf{0}n \rangle \;-\; \langle \mathbf{0}n \,|\, \mathbf{r} \,|\, \mathbf{0}n \rangle^2 \right] \;=\; \sum_n \left[\langle r^2 \rangle_n - \bar{\mathbf{r}}_n^2 \right] \tag{5}$$

as the measure of the spread of the Wannier functions. The sum runs over the n functions $| \mathbf{0}n \rangle$; $\langle r^2 \rangle_n$ and $\bar{\mathbf{r}}_n = \langle \mathbf{r} \rangle_n$ are the expectation values $\langle \mathbf{0}n \,|\, r^2 \,|\, \mathbf{0}n \rangle$ and $\langle \mathbf{0}n \,|\, \mathbf{r} \,|\, \mathbf{0}n \rangle$. Given a set of Bloch orbitals $| \psi_{m\mathbf{k}} \rangle$, the goal is to find the choice of $U_{mn}^{(\mathbf{k})}$ in (3) that minimizes the values of the localization functional (5). We are able to express the gradient $G = \frac{d\Omega}{dW}$

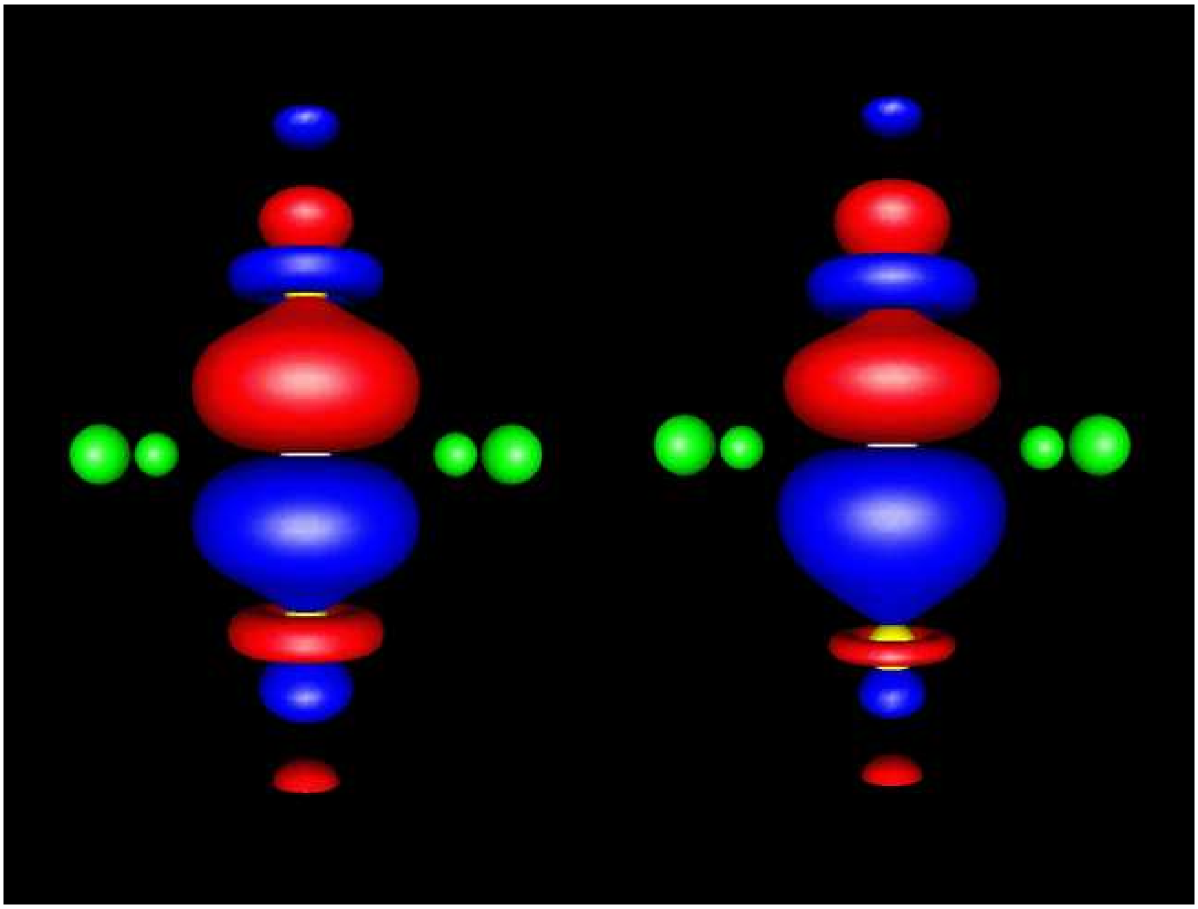

Figure 2: Isosurface contours for a maximally-localized Wannier function in $BaTiO_3$ in the paraelectric (left) and ferroelectric (right) phase. O atoms are in white, Ti yellow, and Ba green. The WF is one of the 9 originating from the composite group of the O $2p$ bands, showing strong and polarizable hybridization between the $2p_z$ orbital of O and the $3d_{z^2}$ orbitals of Ti, usually considered empty in an ionic picture. [From Ref. [19]]

of the localization functional with respect to an infinitesimal unitary rotation of our set of Bloch orbitals

$$|u_{n\mathbf{k}}\rangle \;\rightarrow\; |u_{n\mathbf{k}}\rangle + \sum_m dW^{(\mathbf{k})}_{mn} \, |u_{m\mathbf{k}}\rangle \quad , \tag{6}$$

where dW an infinitesimal antiunitary matrix $dW^\dagger = -dW$ such that

$$U^{(\mathbf{k})}_{mn} = \delta_{mn} + dW^{(\mathbf{k})}_{mn} \quad . \tag{7}$$

This provides an "equation of motion" for the evolution of the $U^{(\mathbf{k})}_{mn}$, and of the $|\,\mathbf{R}n\,\rangle$ derived in (3), towards the minimum of Ω; e.g., in the steepest-descent approach small finite steps in the direction opposite to the gradient decrease the value of Ω, until a minimum is reached. The unitary matrices are then used to construct the Wannier functions via Eq. (3), as illustrated for the semiconductors Si and GaAs in Fig. 1 and for the ferroelectric perovskite $BaTiO_3$ in Fig. 2.

2.1.1 Real-space representation

There are several interesting consequences stemming from the choice of (5) as the localization functional, that we briefly summarize here. Adding and subtracting the off-diagonal components $\widetilde{\Omega} = \sum_n \sum_{\mathbf{R}m \neq \mathbf{0}n} \left| \langle \mathbf{R}m|\mathbf{r}|\mathbf{0}n\rangle \right|^2$, we obtain the decomposition

$$\Omega \,=\, \Omega_{\rm I} \,+\, \widetilde{\Omega} \,=\, \Omega_{\rm I} \,+\, \Omega_{\rm D} \,+\, \Omega_{\rm OD} \tag{8}$$

where $\Omega_{\rm I}$, $\widetilde{\Omega}$, $\Omega_{\rm D}$ and $\Omega_{\rm OD}$ are respectively

$$\Omega_{\rm I} = \sum_n \left[\langle\, \mathbf{0}n \,|\, r^2 \,|\, \mathbf{0}n \,\rangle \,-\, \sum_{\mathbf{R}m} \left| \langle \mathbf{R}m|\mathbf{r}|\mathbf{0}n\rangle \right|^2 \right] , \tag{9}$$

$$\widetilde{\Omega} = \sum_n \sum_{\mathbf{R}m \neq \mathbf{0}n} \left| \langle \mathbf{R}m|\mathbf{r}|\mathbf{0}n\rangle \right|^2 ,$$

$$\Omega_{\rm D} = \sum_n \sum_{\mathbf{R} \neq \mathbf{0}} \left| \langle \mathbf{R}n|\mathbf{r}|\mathbf{0}n\rangle \right|^2 ,$$

$$\Omega_{\rm OD} = \sum_{m \neq n} \sum_{\mathbf{R}} \left| \langle \mathbf{R}m|\mathbf{r}|\mathbf{0}n\rangle \right|^2 .$$

It can be shown that each of these quantities is *positive-definite* (in particular $\Omega_{\rm I}$, see Ref. [17]); moreover, $\Omega_{\rm I}$ is also *gauge-invariant*, i.e., it is invariant under any arbitrary unitary transformation (3) of the Bloch orbitals. The minimization procedure thus corresponds to the minimization of $\widetilde{\Omega} = \Omega_{\rm D} + \Omega_{\rm OD}$. At the minimum, the elements $\left| \langle \mathbf{R}m|\mathbf{r}|\mathbf{0}n\rangle \right|^2$ are as small as possible, realizing the best compromise in the simultaneous diagonalization, within the space of the Bloch bands considered, of the three position operators x, y and z (which do not in general commute when projected within this space).

2.1.2 Reciprocal-space representation

As shown by Blount [18], matrix elements of the position operator between Wannier functions take the form

$$\langle \mathbf{R}n|\mathbf{r}|\mathbf{0}m\rangle = i\, \frac{V}{(2\pi)^3} \int d\mathbf{k}\, e^{i\mathbf{k}\cdot\mathbf{R}} \langle u_{n\mathbf{k}}|\nabla_{\mathbf{k}}|u_{m\mathbf{k}}\rangle \tag{10}$$

and

$$\langle \mathbf{R}n|r^2|\mathbf{0}m\rangle = -\frac{V}{(2\pi)^3} \int d\mathbf{k}\, e^{i\mathbf{k}\cdot\mathbf{R}} \langle u_{n\mathbf{k}}|\nabla^2_{\mathbf{k}}|u_{m\mathbf{k}}\rangle \;\; . \tag{11}$$

These expressions provide the needed connection with our underlying Bloch formalism, since they allow us to express the localization functional Ω in terms of the matrix elements of $\nabla_{\mathbf{k}}$ and $\nabla^2_{\mathbf{k}}$. In addition, they allow us to calculate the effects on the localization of any unitary transformation of the $|u_{n\mathbf{k}}\rangle$ without having to recalculate expensive (at least when plane-wave basis sets are used) scalar products. We thus determine the Bloch orbitals $|u_{m\mathbf{k}}\rangle$ on a regular mesh of $\mathbf{k}$-points, and will use finite differences to evaluate the above derivatives.

To proceed further, we make the assumption throughout this work that the Brillouin zone has been discretized into a uniform Monkhorst-Pack mesh, and the Bloch orbitals determined on that mesh.[1] Let $\mathbf{b}$ be a vector connecting a k-point to one of its near neighbors, and let Z be the number of such neighbors to be included in the finite-difference formulas. We use the simplest possible finite-difference formula for $\nabla_{\mathbf{k}}$, i.e., the one involving the smallest possible Z. When the Bravais lattice point group is cubic, it will only be necessary to include the first shell of $Z = 6$, 8, or 12 k-neighbors for simple cubic, bcc, or fcc k-space meshes, respectively. Otherwise, further shells must be included until it is possible to satisfy the condition

$$\sum_{\mathbf{b}} w_b \, b_\alpha b_\beta = \delta_{\alpha\beta} \tag{12}$$

by an appropriate choice of a weight w_b associated with each shell $|\mathbf{b}| = b$. (For the three kinds of cubic mesh, Eq. (12) is satisfied with $w_b = 3/Zb^2$ and a single shell of 6, 8, or 12 neighbors; even in the worst case of minimal symmetry, only six pairs of neighbors ($Z = 12$) are needed, as the freedom to choose six weights allows one to satisfy the six independent conditions comprising Eq. (12)). Now, if $f(\mathbf{k})$ is a smooth function of $\mathbf{k}$, its gradient can be expressed as

$$\nabla f(\mathbf{k}) = \sum_{\mathbf{b}} w_b \, \mathbf{b} \, [f(\mathbf{k}+\mathbf{b}) - f(\mathbf{k})] \ . \tag{13}$$

In a similar way,

$$|\nabla f(\mathbf{k})|^2 = \sum_{\mathbf{b}} w_b \, [f(\mathbf{k}+\mathbf{b}) - f(\mathbf{k})]^2 \ . \tag{14}$$

It now becomes straightforward to calculate the scalar products involving the reciprocal-space derivatives of Eqs. (10) and (11), since the only elements needed will be the matrix elements between Bloch orbitals at neighboring $\mathbf{k}$-points

$$M_{mn}^{(\mathbf{k},\mathbf{b})} = \langle u_{m\mathbf{k}} | u_{n,\mathbf{k}+\mathbf{b}} \rangle \tag{15}$$

The $M_{mn}^{(\mathbf{k},\mathbf{b})}$ are a central quantity in our formalism, since we will express in their terms all the contributions to the localization functional. After some algebra [17] we can obtain the relevant quantities needed to compute the spread functional, that we report here starting from the center of nth orbital

$$\bar{\mathbf{r}}_n = -\frac{1}{N} \sum_{\mathbf{k},\mathbf{b}} w_b \, \mathbf{b} \, \mathrm{Im} \ln M_{nn}^{(\mathbf{k},\mathbf{b})} \ , \tag{16}$$

to its second moment

$$\langle r^2 \rangle_n = \frac{1}{N} \sum_{\mathbf{k},\mathbf{b}} w_b \left\{ \left[1 - |M_{nn}^{(\mathbf{k},\mathbf{b})}|^2 \right] + \left[\mathrm{Im} \ln M_{nn}^{(\mathbf{k},\mathbf{b})} \right]^2 \right\} \tag{17}$$

[1] Even the case of Γ-sampling – where the Brillouin zone is sampled with a single $\mathbf{k}$-point – is encompassed by the above formulation. In this case the neighboring $\mathbf{k}$-points for Γ are given by the first shell(s) of reciprocal lattice vectors; the Bloch orbitals there differ only by phase factors $\exp(i\mathbf{G} \cdot \mathbf{r})$ from their counterparts at Γ. The algebra does become simpler, though, and will be discussed in a separate section.

and the different terms in the localization functional

$$\Omega_{\mathrm{I}} = \frac{1}{N}\sum_{\mathbf{k},\mathbf{b}} w_b \left(N_{\mathrm{bands}} - \sum_{mn} |M_{mn}^{(\mathbf{k},\mathbf{b})}|^2\right), \tag{18}$$

$$\Omega_{\mathrm{OD}} = \frac{1}{N}\sum_{\mathbf{k},\mathbf{b}} w_b \sum_{m\neq n} |M_{mn}^{(\mathbf{k},\mathbf{b})}|^2, \tag{19}$$

$$\Omega_{\mathrm{D}} = \frac{1}{N}\sum_{\mathbf{k},\mathbf{b}} w_b \sum_{n} \left(-\mathrm{Im}\ \ln M_{nn}^{(\mathbf{k},\mathbf{b})} - \mathbf{b}\cdot\bar{\mathbf{r}}_n\right)^2 \quad . \tag{20}$$

From these, we can calculate the change in the localization functional in response to an infinitesimal unitary transformation of the Bloch orbitals as a function of the $M_{mn}^{(\mathbf{k},\mathbf{b})}$; once these gradients are available, it is straightforward to construct a procedure that updates the $U_{mn}^{(\mathbf{k})}$ (and consequently the $M_{mn}^{(\mathbf{k},\mathbf{b})}$) towards the minimum localization.

3 Localization procedure

We now consider the first-order change of the spread functional Ω arising from an infinitesimal gauge transformation, given by $U_{mn}^{(\mathbf{k})} = \delta_{mn} + dW_{mn}^{(\mathbf{k})}$, where dW is an infinitesimal antiunitary matrix, $dW^\dagger = -dW$, so that $|u_{n\mathbf{k}}\rangle \rightarrow |u_{n\mathbf{k}}\rangle + \sum_m dW_{mn}^{(\mathbf{k})}\,|u_{m\mathbf{k}}\rangle$. We seek an expression for $d\Omega/dW_{mn}^{(\mathbf{k})}$. We use the convention

$$\left(\frac{d\Omega}{dW}\right)_{nm} = \frac{d\Omega}{dW_{mn}} \tag{21}$$

(note the reversal of indeces) and introduce $\mathcal{A}$ and $\mathcal{S}$ as the superoperators $\mathcal{A}[B] = (B - B^\dagger)/2$ and $\mathcal{S}[B] = (B + B^\dagger)/2i$. Defining

$$q_n^{(\mathbf{k},\mathbf{b})} = \mathrm{Im}\ \ln M_{nn}^{(\mathbf{k},\mathbf{b})} + \mathbf{b}\cdot\bar{\mathbf{r}}_n \tag{22}$$

$$R_{mn}^{(\mathbf{k},\mathbf{b})} = M_{mn}^{(\mathbf{k},\mathbf{b})} M_{nn}^{(\mathbf{k},\mathbf{b})*} \ \ ; \ \ \widetilde{R}_{mn}^{(\mathbf{k},\mathbf{b})} = \frac{M_{mn}^{(\mathbf{k},\mathbf{b})}}{M_{nn}^{(\mathbf{k},\mathbf{b})}} \ \ ; \ \ T_{mn}^{(\mathbf{k},\mathbf{b})} = \widetilde{R}_{mn}^{(\mathbf{k},\mathbf{b})} q_n^{(\mathbf{k},\mathbf{b})} \quad . \tag{23}$$

and referring to Ref. [17] for the details, we arrive at the explicit expression for the gradient of the spread functional

$$G^{(\mathbf{k})} = \frac{d\Omega}{dW^{(\mathbf{k})}} = 4\sum_{\mathbf{b}} w_b \left(\mathcal{A}[R^{(\mathbf{k},\mathbf{b})}] - \mathcal{S}[T^{(\mathbf{k},\mathbf{b})}]\right) \quad . \tag{24}$$

In order to minimize the spread functional Ω by steepest descents, we make small updates to the unitary matrices, as in Eq. (7), choosing

$$dW^{(\mathbf{k})} = \epsilon\, G^{(\mathbf{k})}$$

where ϵ is a positive infinitesimal. We then have, to first order in ϵ,

$$d\Omega = \sum_{\mathbf{k}} \mathrm{tr}\,[G^{(\mathbf{k})} dW^{(\mathbf{k})}] = -\epsilon \sum_{\mathbf{k}} \|G^{(\mathbf{k})}\|^2 \ , \tag{25}$$

In practice, we take a fixed finite step $\Delta W^{(\mathbf{k})}$, and the wavefunctions are then updated according to the matrix $\exp[\Delta W^{(\mathbf{k})}]$, which is unitary since ΔW is antihermitian. The matrix $\exp[\Delta W^{(\mathbf{k})}]$ can be straightforwardly constructed from the eigenvalues and eigenvectors of $i\Delta W^{(\mathbf{k})}$, that is a regular Hermitian matrix.[2] More efficient minimization strategies should be used when dealing with large systems or very fine k-point meshes (e.g., conjugate-gradients minimizations).

It should be stressed that the evolution towards the minimum requires only the relatively inexpensive updating of the unitary matrices, and not of the wavefunctions. We start from a reference set of Bloch orbitals $|u^{(0)}_{n\mathbf{k}}\rangle$ obtained in our first-principles calculation, and compute once and for all the

$$M^{(0)(\mathbf{k},\mathbf{b})}_{mn} = \langle u^{(0)}_{m\mathbf{k}} | u^{(0)}_{n,\mathbf{k}+\mathbf{b}} \rangle \ . \tag{26}$$

We then represent the $|u_{n\mathbf{k}}\rangle$ (and thus, indirectly, the Wannier functions) in terms of the $|u^{(0)}_{n\mathbf{k}}\rangle$ and a set of unitary matrices $U^{(\mathbf{k})}_{mn}$,

$$|u_{n\mathbf{k}}\rangle = \sum_m U^{(\mathbf{k})}_{mn} \, |u^{(0)}_{m\mathbf{k}}\rangle \ . \tag{27}$$

We begin with all the $U^{(\mathbf{k})}_{mn}$ initialized to δ_{mn}. Then, each step of the steepest-descent procedure involves calculating ΔW for a small step in the direction opposite to the gradient, updating the unitary matrices according to

$$U^{(\mathbf{k})} \ \rightarrow \ U^{(\mathbf{k})} \, \exp[\Delta W^{(\mathbf{K})}] \ , \tag{28}$$

and then computing a new set of M matrices according to

$$M^{(\mathbf{k},\mathbf{b})} = U^{(\mathbf{k})\dagger} \, M^{(0)(\mathbf{k},\mathbf{b})} \, U^{(\mathbf{k}+\mathbf{b})} \ . \tag{29}$$

In the most general case, the localization functional can display artificial "unphysical" local minima; to avoid these, we typically prepare a set of reference Bloch orbitals $|u^{(0)}_{n\mathbf{k}}\rangle$ by projection from a set of initial trial orbitals $g_n(\mathbf{r})$ corresponding to some very rough initial guess $g_n(\mathbf{r})$ for the Wannier functions. The $g_n(\mathbf{r})$ are projected onto the Bloch manifold at wavevector $\mathbf{k}$,

$$|\phi_{n\mathbf{k}}\rangle = \sum_m |\psi_{m\mathbf{k}}\rangle\langle\psi_{m\mathbf{k}}|g_n\rangle \ , \tag{30}$$

are orthonormalized via the Löwdin transformation

$$|\widetilde{\phi}_{n\mathbf{k}}\rangle = \sum_m (S^{-1/2})_{mn} |\phi_{m\mathbf{k}}\rangle \tag{31}$$

[2] The unitary matrix $\exp(W)$ is obtained diagonalizing $H = iW$: since W is anti-Hermitian, H is Hermitian and has real eigenvalues ϵ_l and eigenvectors Z_{mn} such that $\epsilon_l = \sum_{mn} Z_{lm} H_{mn} Z^\dagger_{nl}$; then $(\exp(W))_{lm}$ is given by $\sum_n Z^\dagger_{ln} \exp(-i\epsilon_n) Z_{nm}$.

(where $S_{mn} = \langle \phi_{m\mathbf{k}} | \phi_{n\mathbf{k}} \rangle$), and finally reconverted to cell-periodic functions with

$$u^{(0)}_{n\mathbf{k}}(\mathbf{r}) = e^{-i\mathbf{k}\cdot\mathbf{r}} \widetilde{\phi}_{n\mathbf{k}}(\mathbf{r}) \quad . \tag{32}$$

We then use this set of reference Bloch orbitals as a starting point for the minimization procedure.

4 Two limiting cases: Isolated systems and large supercells

The formulation introduced above can be significantly simplified in two important cases, which merit a separate discussion. (i) When open boundary conditions are used instead of periodic boundary conditions; this is appropriate for treating finite, isolated systems (e.g., molecules and clusters) using localized basis sets, and is the standard approach in quantum chemistry. In this case the localization procedure can be entirely recast in real space, and corresponds to determining Boys localized orbitals of quantum chemistry. (ii) When the system studied can be described using a large periodic supercell. This is the case of amorphous solids or liquids; finite systems can also be described in this way, using large enough supercells so as to eliminate the interactions with periodic images. The Brillouin zone of a large supercell is sufficiently small that integrations over $\mathbf{k}$-vectors can be substituted with single-point sampling at its center (the Γ point).

4.1 Real-space formulation

We describe first the real-space localization procedure, changing notation $|\mathbf{R}n\rangle \rightarrow |w_i\rangle$ to refer to the orbitals of the isolated system that will become maximally localized. We decompose again the localization functional $\Omega = \sum_i [\langle r^2 \rangle_i - \bar{\mathbf{r}}_i^2]$ into an invariant part $\Omega_{\mathrm{I}} = \sum_\alpha \mathrm{tr}\,[P r_\alpha Q r_\alpha]$ (where $P = \sum_i |w_i\rangle\langle w_i|$, $Q = \mathbf{1} - P$, and 'tr' refers to a sum over all the states w_i) and a remainder $\widetilde{\Omega} = \sum_\alpha \sum_{i \neq j} |\langle w_i | r_\alpha | w_j \rangle|^2$ that needs to be minimized. Defining the matrices $X_{ij} = \langle w_i | x | w_j \rangle$, $X_{\mathrm{D},ij} = X_{ij}\,\delta_{ij}$, $X' = X - X_{\mathrm{D}}$, and similarly for Y and Z, $\widetilde{\Omega}$ can be rewritten as

$$\widetilde{\Omega} = \mathrm{tr}\,[X'^2 + Y'^2 + Z'^2] \quad . \tag{33}$$

If X, Y, and Z could be simultaneously diagonalized, then $\widetilde{\Omega}$ could be minimized to zero (leaving only the invariant part); for non-commuting matrices this is not generally possible (although one could choose, as in [24], a preferred direction of localization). Our task is then to perform the optimal approximate simultaneous co-diagonalization of the three Hermitian matrices X, Y, and Z by a single unitary transformation. Although a formal solution for this problem is missing, implementing a numerical minimization (e.g., by steepest-descents or conjugate-gradient, see below) is fairly straightforward. This problem appears also in the context of multivariate analysis [25] and signal processing [26], and has been recently revisited in relation with the present localization approach [27] (see also Sec. IIIA in Ref. [28]). Since $\mathrm{tr}\,[X' X_{\mathrm{D}}] = 0$, etc.,

$$d\Omega = 2\,\mathrm{tr}\,[X' dX + Y' dY + Z' dZ] \quad . \tag{34}$$

We then consider an infinitesimal unitary transformation $|w_i\rangle \rightarrow |w_i\rangle + \sum_j W_{ji}|w_j\rangle$ (where dW is antihermitian), from which $dX = [X, dW]$, etc. Inserting in Eq. (34) and using $\mathrm{tr}\,[A[B,C]] = \mathrm{tr}\,[C[A,B]]$ and $[X', X] = [X', X_\mathrm{D}]$, we obtain $d\Omega = \mathrm{tr}\,[dW\, G]$ where

$$G = 2\Big\{[X', X_\mathrm{D}] + [Y', Y_\mathrm{D}] + [Z', Z_\mathrm{D}]\Big\} \ , \tag{35}$$

so that the desired gradient is $d\Omega/dW = G$ as given above. The minimization can then be carried out using the general approach already outlined.

4.2 Γ-point formulation

With an appropriate redefinition of the quantities X_{ij}, a similar formulation applies in reciprocal space when dealing with isolated or very large systems in periodic boundary conditions, i.e., whenever it becomes appropriate to sample the wavefunctions only at the Γ-point of the Brillouin zone.

We start with the simpler case for a calculation in a cubic supercell of side L, following the derivation of Ref. [29]. The maximum-localization criterion turns out to be equivalent (see Eq. (41) below) to the problem of maximizing the functional

$$\Xi = \sum_{n=1}^{N} \left(|X_{nn}|^2 + |Y_{nn}|^2 + |Z_{nn}|^2\right) \ , \tag{36}$$

where $X_{mn} = \langle w_m | e^{-i\frac{2\pi}{L}x} | w_n\rangle$ (similar definitions for Y_{mn} and Z_{mn} apply). Once the gradient of this functional is determined, its maximization can be performed using again a steepest-descent algorithm.[3] Some simple algebra shows that the gradient $d\Xi/dA_{mn}$ is given by the sum of $[X_{nm}(X^*_{nn} - X^*_{mm}) - X^*_{mn}(X_{mm} - X_{nn})]$ and the equivalent terms with Y and Z substituted in place of X. We this start the procedure by constructing new matrices $X^{(1)}$, $Y^{(1)}$ and $Z^{(1)}$ via the unitary transformations $X^{(1)} = \exp(-A^{(1)})X^{(0)}\exp(A^{(1)})$ (and similarly for $Y^{(1)}$ and $Z^{(1)}$), where $X^{(0)}_{mn} = \langle w^{(0)}_m | e^{-i\frac{2\pi}{L}x} | w^{(0)}_n\rangle$ and $w^{(0)}_n(\mathbf{r}) = \psi_n(\mathbf{r})$ are the Kohn-Sham (KS) orbitals obtained after a conventional electronic structure calculation. $A^{(1)}$ is an $\mathbf{N} \times \mathbf{N}$ antihermitian matrix corresponding to a finite step in the direction of the gradient of Ξ with respect to all the possible unitary transformations given by $\exp(-A)$: $A^{(1)} = \lambda\,(d\Xi/dA)^{(0)}$, where λ is the length of the steepest-descent step. This process is repeated up to convergence in the Ξ functional – as always, more sophisticated algorithms can be used (e.g., introducing line searches along λ, or conjugate-gradient strategies). At the end of the iterative procedure, the maximally-localized Wannier functions are then given by the unitary rotation

$$w_n(\mathbf{r}) = \sum_m \left[\Pi_i \exp(-A^{(i)})\right]_{mn} \psi_m(\mathbf{r}) \tag{37}$$

[3] Note that in the limit of a single k point the distinction between Bloch orbitals and Wannier functions becomes irrelevant, since no Fourier transform from $\mathbf{k}$ to $\mathbf{R}$ is involved in the transformation (37); rather, we want to find the optimal unitary matrix that rotates the ground-state self-consistent orbitals into their maximally-localized representation.

of the original N orbitals. The coordinate x_n of the n-th Wannier-function center (WFC) is computed using the formula

$$x_n = -\frac{L}{2\pi} \operatorname{Im} \ln \langle w_n | e^{-i\frac{2\pi}{L}x} | w_n \rangle \ , \tag{38}$$

with similar definitions for y_n and z_n. Eq. (38) has been shown by Resta to be the correct definition of the expectation value of the position operator for a system with periodic boundary conditions, and had been introduced several years ago to deal with the problem of determining the average position of a single electronic orbital in a periodic supercell [30]. The computational effort required in Eqs. (36) and (38) is negligible, once the scalar products needed to construct the initial $X^{(0)}$, $Y^{(0)}$ and $Z^{(0)}$ have been calculated.

The extension to supercells of arbitrary symmetry has been derived by Silvestrelli [31]. By defining overlap matrices

$$M^l_{mn} = \langle w_m | e^{-i\mathbf{G}_l \cdot \mathbf{r}} | w_n \rangle, \tag{39}$$

(where $\mathbf{G}_l$ are the reciprocal lattice vectors of the unit cell, w_j is the Wannier functions), a functional Ξ is defined as

$$\Xi = \sum_{n=1}^{N} \sum_{l=1}^{N_G} W_l \, |M^l_{nn}|^2 \tag{40}$$

(N_G is the number of the $\mathbf{G}_l$ vectors used, and W_l is the weight corresponding to the vector G_l). This functional is closely related to the spread of the Wannier functions:

$$\begin{aligned} \Omega &= \left(\frac{L}{2\pi}\right)^2 \sum_{n=1}^{N} \sum_{l=1}^{N_G} W_l \left[\langle w_n | (\mathbf{G}_l \cdot \mathbf{r})^2 | w_n \rangle - \langle w_n | \mathbf{G}_l \cdot \mathbf{r} | w_n \rangle^2 \right] \\ &= \left(\frac{L}{2\pi}\right)^2 \sum_{n=1}^{N} \sum_{l=1}^{N_G} W_l \left(1 - |\langle w_n | e^{-i\mathbf{G}_l \cdot \mathbf{r}} | w_n \rangle|^2 \right) + O(L^{-2}) \\ &= \left(\frac{L}{2\pi}\right)^2 \left(\sum_{n=1}^{N} \sum_{l=1}^{N_G} W_l \, - \Xi \right) + O(L^{-2}) \ , \end{aligned} \tag{41}$$

where L is the supercell dimension. Thus, instead of minimizing the spread, we maximize the functional Ξ to retrieve the MLWFs. The Wannier function center of the n'th occupied band, $\mathbf{r}_n$, can be computed from

$$\mathbf{r}_n = -\left(\frac{L}{2\pi}\right)^2 \sum_l W_l \, \mathbf{G}_l \operatorname{Im} \ln M^l_{nn}. \tag{42}$$

Care should be taken when comparing the spreads of MLWFs calculated in supercells of different sizes. Even for the ideal case of an isolated molecule, the Wannier centers and the general shape of the MLWFs will rapidly reach their exact limit as the cell size is increased. On the other hand, the numerical value for the total spread Ω will display much slower convergence. This behavior derives from the finite-difference representation of the invariant part of the localization functional (essentially, it's a second derivative); while Ω_I

does not contribute to the localization properties of the MLWFs, it does numerically add up in the evaluation of the spreads, and usually represents the largest term. This slow convergence had already been noted in the original work [17] when commenting on the convergence properties of Ω with respect to the spacing of the Monkhorst-Pack mesh.

5 Entangled bands

In the case of bulk materials, the methods described in the previous sections were designed with *isolated* groups of bands in mind. By this we mean a group of bands that may become degenerate with one another at certain symmetry points or lines in the Brillouin zone (composite bands), but are separated from all other bands by finite gaps throughout the entire Brillouin zone (in the case of disordered systems it is more appropriate to think in terms of a gap in the density of states). The valence bands of insulators are the most important example, and indeed these methods have been applied mostly to insulating materials. However, in some applications the bands of interest are not isolated. This is the case when studying electron transport in metals, which is governed by the partially filled bands close to the Fermi level. The four low-lying antibonding bands of a tetrahedral semiconductor, which are connected to higher conduction bands, provide another example. In both cases the desired bands lie within a limited energy range but cross with, or are attached to, other bands which extend further out in energy. We will refer to them as *entangled* bands.

The difficulty in treating entangled bands stems from the fact that it is unclear exactly which N bands to choose, particularly in those regions of k space where the bands of interest are hybridized with unwanted bands. Before the Wannier-localization methods can be applied, some prescription is needed to extract N states per k point from the entangled manifold.

We have recently developed a strategy [32] that achieves this goal with minimal user intervention. Once an N-dimensional manifold has been obtained at each k, the usual localization procedure, based on minimizing $\widetilde{\Omega}$, can be used to generate the maximally-localized Wannier functions for that manifold. The problem of computing well-localized Wannier functions starting from entangled bands is then broken down into two distinct steps. The new feature is the first step (disentangling of the bands, or subspace selection), which is outlined below, while the second step is the same as for isolated groups of bands.

5.1 The disentangling procedure

5.1.1 Method

For definiteness let us suppose we want to disentangle the five d bands of copper from the s band which crosses them (see Fig. 3) and construct a set of well-localized WFs associated with the resulting d bands. Heuristically the d bands are the five narrow bands

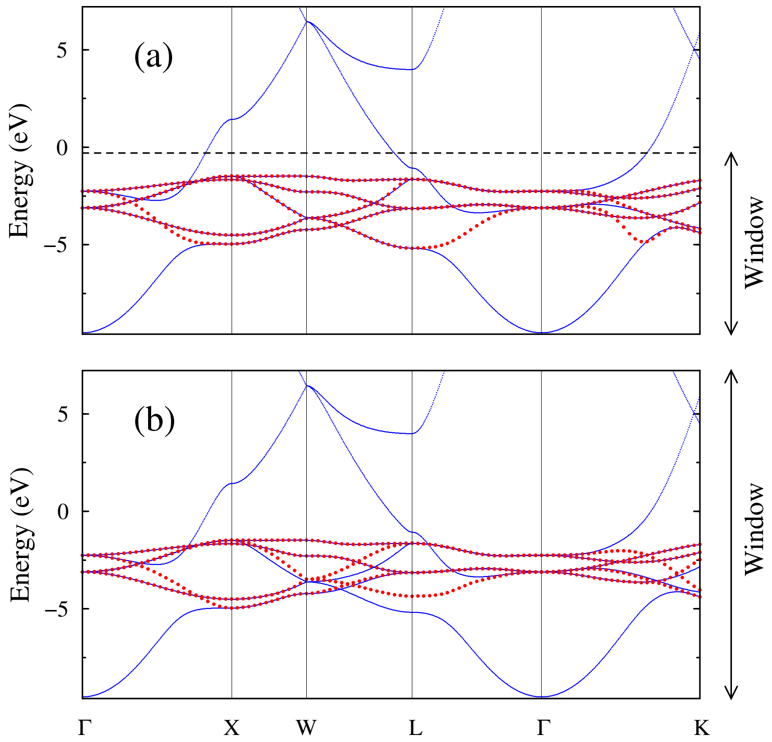

Figure 3: Blue lines: Calculated band structure of copper. Red lines: Interpolated bands obtained from the five d-like Wannier functions. (a) and (b) differ in the choice of energy window used in the disentangling step. [From Ref. [32]]

and the s band is the wide band. The difficulty arises because there are regions of k-space where all six bands are close together, so that as a result of hybridization the distinction between d-band and s-band levels is not meaningful.

First we cut out an energy window that encompasses the N bands of interest ($N = 5$ in our example). Figs. 3(a) and 3(b) correspond to different choices for this energy window. At each k-point the number $N_{\mathbf{k}}$ of bands that fall inside the window is equal to or larger than the target number of bands N. This procedure defines an $N_{\mathbf{k}}$-dimensional projective Hilbert space $\mathcal{F}(\mathbf{k})$ spanned by the eigenstates $|u_{n\mathbf{k}}\rangle$ within the window at some $\mathbf{k}$. If $N_{\mathbf{k}} = N$, there is nothing to do there; if $N_{\mathbf{k}}\rangle N$ our aim is to find the N-dimensional subspace $\mathcal{S}(\mathbf{k}) \subseteq \mathcal{F}(\mathbf{k})$ that, among all possible N-dimensional subspaces of $\mathcal{F}(\mathbf{k})$, leads to the smallest Ω_{I} [Eq. (18)]. Recall that for an isolated group of bands Ω_{I} is gauge-invariant, since it is an intrinsic property of the manifold of states. Thus Ω_{I} can be regarded as a functional of $\mathcal{S}(\mathbf{k})$. In practice $\mathcal{S}(\mathbf{k})$ is specified by an orthonormal set of N *pseudo*-Bloch states $|\widetilde{u}_{n\mathbf{k}}\rangle$, so that $\Omega_{\mathrm{I}} = \Omega_{\mathrm{I}}(\{\widetilde{u}_{n\mathbf{k}}\})$. We will then apply the procedure of Sec. 3 to the manifold of states $\mathcal{S}(\mathbf{k})$ in order to obtain a set of MLWFs spanning this space (see Fig. 4 for the MLWFs resulting from the disentangled d bands of copper).

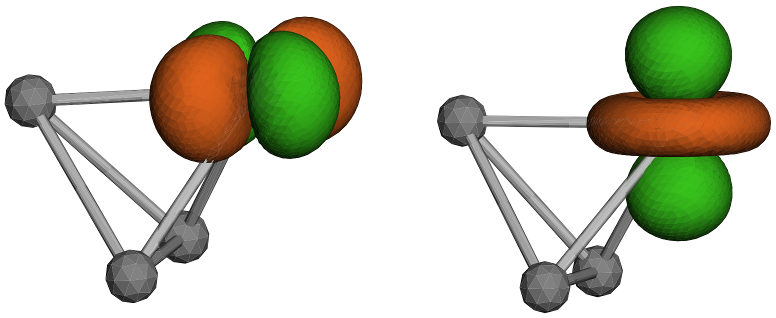

Figure 4: Contour-surface plots of the two e_g Wannier functions associated with the disentangled d bands of copper shown in Fig. 3. The amplitudes are $+0.5/\sqrt{v}$ (green) and $-0.5/\sqrt{v}$ (orange), where v is the volume of the primitive cell. [From Ref. [32]]

5.1.2 Rationale

Why is minimizing $\Omega_{\rm I}(\{\widetilde{u}_{n\mathbf{k}}\})$ a sensible strategy for picking out the d-bands? This can be understood by noting that $\Omega_{\rm I}$ heuristically measures the change of character of the states across the Brillouin zone. Indeed, Eq. (18) shows that $\Omega_{\rm I}$ is small whenever $|\langle\widetilde{u}_{n\mathbf{k}}|\widetilde{u}_{m,\mathbf{k}+\mathbf{b}}\rangle|^2$, the square of the magnitude of the overlap between states at nearby k-points, is large. Thus by minimizing $\Omega_{\rm I}$ we are choosing self-consistently at every $\mathbf{k}$ the subspace $\mathcal{S}(\mathbf{k})$ that changes as little as possible with $\mathbf{k}$, i.e., has minimum "spillage" or mismatch with neighboring subspaces. In the present example this maximal "global smoothness of connection" will be achieved by keeping the five well-localized d-like states and excluding the more delocalized s-like state. This can be understood from the fact that $\Omega_{\rm I}$ is a measure of real-space localization, a property that correlates with smoothness in k space.

What is meant by spillage becomes clear once we rewrite Eq. (18) for $\Omega_{\rm I}(\{\widetilde{u}_{n\mathbf{k}}\})$ as

$$\Omega_{\rm I} = \frac{1}{N_{\rm kp}} \sum_{\mathbf{k},\mathbf{b}} w_b \, T_{\mathbf{k},\mathbf{b}} \tag{43}$$

with

$$T_{\mathbf{k},\mathbf{b}} = {\rm tr}[\hat{P}_{\mathbf{k}} \, \hat{Q}_{\mathbf{k}+\mathbf{b}}], \tag{44}$$

where $\hat{P}_{\mathbf{k}} = \sum_n |\widetilde{u}_{n\mathbf{k}}\rangle\langle\widetilde{u}_{n\mathbf{k}}|$ is the projector onto $\mathcal{S}(\mathbf{k})$, $\hat{Q}_{\mathbf{k}} = \mathbf{1} - \hat{P}_{\mathbf{k}}$, and the indeces m,n run over $1,\ldots,N$. $T_{\mathbf{k},\mathbf{b}}$ is called the spillage between the spaces $\mathcal{S}(\mathbf{k})$ and $\mathcal{S}(\mathbf{k}+\mathbf{b})$ because it measures the degree of mismatch between them, vanishing when they are identical.

5.1.3 Numerical algorithm

The minimization of $\Omega_{\rm I}$ inside an energy window is conveniently done using an algebraic algorithm. The stationarity condition $\delta\Omega_{\rm I}(\{\widetilde{u}_{n\mathbf{k}}\}) = 0$, subject to orthonormality constraints, is equivalent to solving the set of eigenvalue equations

$$\Big[\sum_{\mathbf{b}} w_b\, \hat{P}_{\mathbf{k}+\mathbf{b}}\Big]\, |\widetilde{u}_{n\mathbf{k}}\rangle = \lambda_{n\mathbf{k}}\, |\widetilde{u}_{n\mathbf{k}}\rangle\ . \tag{45}$$

Clearly these equations, one for each k point, are coupled, so that the problem has to be solved self-consistently throughout the Brillouin zone. Our strategy is to proceed iteratively until the maximal "global smoothness of connection" is achieved. On the i-th iteration we go through all the k-points in the grid, and for each of them we find N orthonormal states $\left|\widetilde{u}^{(i)}_{n\mathbf{k}}\right\rangle$, defining a subspace $\mathcal{S}^{(i)}(\mathbf{k}) \subseteq \mathcal{F}(\mathbf{k})$ such that the spillage over the neighboring subspaces $\mathcal{S}^{(i-1)}(\mathbf{k}+\mathbf{b})$ from the previous iteration is as small as possible. In this iterative formulation one solves at each step the set of equations

$$\Big[\sum_{\mathbf{b}} w_b\, \hat{P}^{(i-1)}_{\mathbf{k}+\mathbf{b}}\Big] \left|\widetilde{u}^{(i)}_{n\mathbf{k}}\right\rangle = \lambda^{(i)}_{n\mathbf{k}} \left|\widetilde{u}^{(i)}_{n\mathbf{k}}\right\rangle\ . \tag{46}$$

When constructing $\mathcal{S}^{(i)}(\mathbf{k})$ one should pick the N eigenvectors of Eq. (45) with largest eigenvalues, since that choice ensures that at self-consistency the stationary point corresponds to the absolute minimum of Ω_{I}. Self-consistency is achieved when $\mathcal{S}^{(i)}(\mathbf{k}) = \mathcal{S}^{(i-1)}(\mathbf{k})$ at all the grid points. We have encountered cases where the iterative procedure outlined above was not stable. In those cases, the problem was solved by using as the input for each step a linear mixing of the input and output subspaces from the previous step.

In practice we solve Eq. (46) in the basis of the original $N_{\mathbf{k}}$ Bloch eigenstates $|u_{n\mathbf{k}}\rangle$ inside the energy window. Each iteration then amounts to diagonalizing the following $N_{\mathbf{k}} \times N_{\mathbf{k}}$ Hermitian matrix at every $\mathbf{k}$:

$$Z^{(i)}_{mn}(\mathbf{k}) = \Big\langle u_{m\mathbf{k}}\Big| \sum_{\mathbf{b}} w_b \left[\hat{P}^{(i-1)}_{\mathbf{k}+\mathbf{b}}\right]_{\mathrm{in}} \Big|u_{n\mathbf{k}}\Big\rangle. \tag{47}$$

Since these are small matrices, each step of the iterative procedure is computationally inexpensive. The most time-consuming part of the algorithm is the computation of the overlap matrices $M^{(\mathbf{k},\mathbf{b})}$. We stress that all $M^{(\mathbf{k},\mathbf{b})}$ are computed once and for all at the beginning of the Wannier postprocessing, using the original Bloch eigenstates inside the energy window [Eq. (26)]; all subsequent operations in the iterative minimization of Ω_{I} involve only dense linear algebra on small $N_{\mathbf{k}} \times N_{\mathbf{k}}$ matrices. (An analogous situation occurs during the minimization of $\widetilde{\Omega}$ to obtain the MLWFs: see Eqs. (28)-(29).)

As indicated above, having selected the maximally-connected N-dimensional subspaces $\mathcal{S}(\mathbf{k})$, in a second step we work within those subspaces and minimize $\widetilde{\Omega}$ using the same algorithm as for isolated groups of bands. The end result is a set of N maximally-localized WFs and the corresponding N energy bands (red lines in Fig. 3), which are computed from the WFs using an interpolation scheme.

Since in each step we have separately minimized the two terms, Ω_{I} and $\widetilde{\Omega}$, comprising the total Wannier spread Ω, we can regard the resulting orbitals as the N most-localized Wannier functions that can be obtained using states inside the energy window. It should be understood that the Bloch-like states $|\widetilde{u}_{n\mathbf{k}}\rangle$ spanning the optimal subspaces $\mathcal{S}(\mathbf{k})$ do not simply correspond, by unitary rotation, to a subset of the Bloch eigenstates inside the window. Accordingly, the associated N energy bands do not reproduce exactly any subset of the original bands throughout the Brillouin zone. The differences are more pronounced where hybridization with unwanted bands in the original band structure was the strongest. The disentangling procedure can be easily modified [32] so that inside a second ("inner") energy window the original Bloch states – and hence the original bands – are exactly reproduced. The result of such a procedure is illustrated in Fig. 5 for copper. The two-window technique has been applied recently to electromagnetic bands in photonic crystals [15].

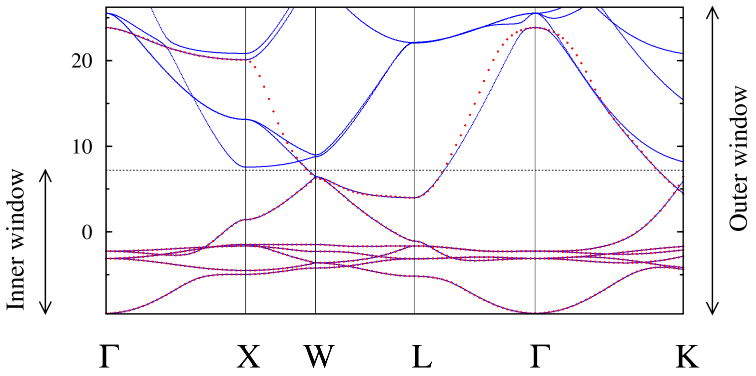

Figure 5: Blue lines: Calculated band structure of copper. Red lines: Interpolated bands for the maximally-connected seven-dimensional subspace using both an "outer" and an "inner" energy window. Inside the latter window the original and interpolated bands are identical. [From Ref. [32]]

6 Discussion

6.1 Alternative localization criteria

Even after the non-uniqueness of the Wannier functions is resolved (in our case by fixing all the gauge freedoms via the constraint of minimal quadratic spread), we are still left with an indeterminacy that follows from the existence of *different* plausible localization criteria. Other measures of localization have been used in the chemistry literature besides the most popular one of Boys [7]. For example, the Coulomb self-repulsion can be maximized, as in the Edmiston-Ruedenberg approach [33], or the projection on a Mulliken population, as in the Pipek-Mezey approach [34]. No matter which criterion is used, the vector sum of all Wannier centers over a primitive cell remains gauge-invariant, so that the connection to the macroscopic polarization is equally true for all localization criteria. However, the individual charge centers [35], the shapes, and even the symmetries of the Wannier functions may depend upon the choice of gauge (or of the choice of localization criterion that leads to the choice of gauge).

For isolated molecules, there is a slight theoretical preference for the Edmiston-Ruedenberg criterion, due to its ability to clearly separate σ- and π-like orbitals in double bonds. (The Boys criterion often mixes the two into so-called "banana" orbitals [34].) A well-known and most severe problem is the description of carbon dioxide (at least if the traditional O=C=O Lewis picture is upheld), where the Boys criterion leads to two triple bonds between the carbon and the oxygen, and one lone pair on each oxygen [36]. (We note in passing that this is actually reminiscent of CO_2 being a resonance structure between two states O≡C-O and O-C≡O.) On the other hand, the Boys criterion leads, in almost all other cases, to orbitals that are very similar to the Edmiston-Ruedenberg ones, and at a much reduced cost (cubic vs. quintic scaling with system size). It would be useful to carry out similar investigations comparing the use of different localization criteria in solids, but to our knowledge there have been no direct studies along these lines.

Nevertheless, we lean towards the view that in most cases the use of any "reasonable" localization criterion will lead to rather similar MLWFs that give a qualitatively and semiquantitatively similar description of the system of interest. The fact that the Boys and Edmiston-Ruedenberg MLWFs are usually so similar supports this viewpoint. Further support comes from the fact that we have seen very little difference in our results (especially when considering systems with high symmetry) when even simple projection techniques have been used [37, 12], along the lines of Eq. (30), without doing afterwards an actual minimization. For the case of silicon, localized orbitals very similar to our MLWFs have been obtained using a linear-scaling functional [38] that constrains the spread of an orbital inside a support region of finite (small) radius.

We report here the case case of high-pressure hydrogen, a molecular solid that shows significant infrared activity arising from overlap between the constituent molecules. In particular, we looked at the individual dipoles of the MLWFs in an attempt to extract from them useful physical information. An initial guess was made for the localized WFs with the help of trial functions which are bond-centered Gaussians (we will call the resulting orbitals "projected WFs"). Their localization was then refined by actually minimizing the quadratic spread Ω yielding the MLWFs. Since the projected WFs are totally oblivious to the localization criterion that one uses later to localize them further, it seems reasonable to assume that the difference between the projected and the MLWFs is an *upper bound* to the differences that would occur between WFs obtained using any two sensible localization criteria.

We show in Fig. 6 the results, for the solid in the $Cmc2_1$ structure at a density of $r_s = 1.52$, for which the average r.m.s. width of the MLWFs is $\overline{\lambda} = 1.11$ a.u. If we choose the r.m.s. width of the initial bond-centered Gaussians to be 1.89 a.u. (1 Å), the resulting projected WFs are essentially indistinguishable from the MLWFs. For instance, the curves corresponding to those in Fig. 6 are virtually identical, and the individual Wannier dipoles remain the same to at least six significant digits! This is compelling evidence for a high degree of uniqueness of well-localized WFs in this system, at least for our high-symmetry configurations. If we were to double the width of the initial Gaussian, some differences

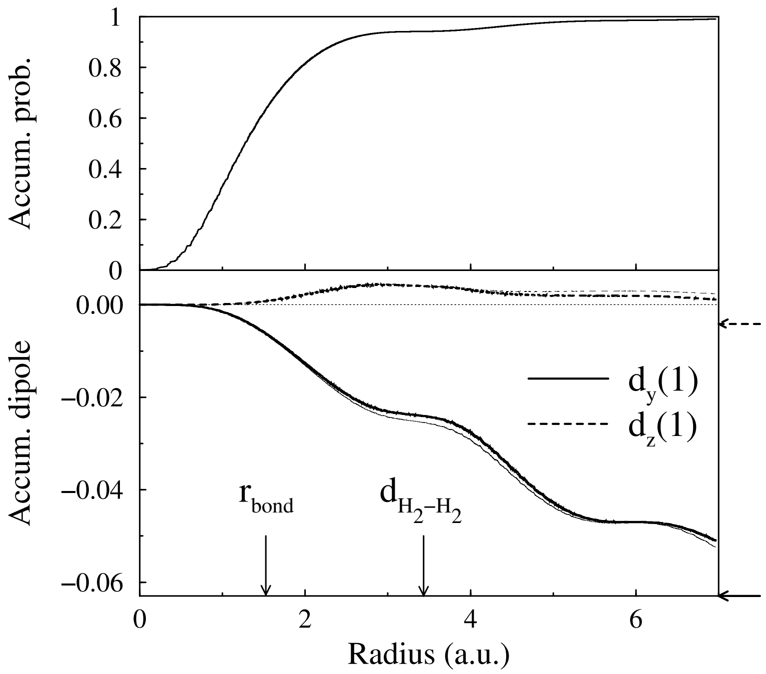

Figure 6: Upper panel: accumulated radial integral of the square of the MLWFs of an hydrogen molecule in the dense solid, $\int_{|\mathbf{r}|\langle r_0} |w_1(\mathbf{r})|^2 d\mathbf{r}$, as a function of r_0, for $Cmc2_1$ at $r_s = 1.52$; the integral starts at the molecular center and converges to one for large r_0. Lower panel, thick lines: accumulated radial integral of the Cartesian components of the Wannier dipole moment, $-2e \int_{|\mathbf{r}|\langle r_0} \mathbf{r}|w_1(\mathbf{r})|^2 d\mathbf{r}$ (the x-component vanishes by symmetry for all r_0); the arrows denote the converged values. The thin lines correspond to the WF obtained from bond-centered Gaussians with a r.m.s. width of 2.0 Å. [From Ref. [37]]

would start to appear. These are barely visible in the accumulated radial integral of the probability (see Fig. 6) but become noticeable, although still relatively small, in the radially integrated dipole (lower panel of Fig. 6). For instance, the large y-component of the dipole changes by around 2% (in $Cmc2_1$ the z-component is fixed by symmetry: $d_z(n) = v(P_{\rm mac})_z/2$, where $n = 1, 2$ labels the molecule in the primitive cell).

The dielectric decomposition of the charge density of an extended system into well-defined Wannier dipoles was first introduced for the case of liquid water by Silvestrelli and Parrinello [39]. Such analysis offers an enlightening picture of the electronic properties of a disordered system that wouldn't otherwise be available from the charge density alone, or from the eigenstates of the Hamiltonian. For the case of water a study was performed [40] spanning the phase diagram at intermediate steps between normal and supercritical conditions. Close to the low-density supercritical point there appears a shift in the average value for the Wannier dipoles, from a value around ~ 3 Debye under normal conditions (this is a typical value for liquid water [41]) to a much lower value close to the supercritical point, approaching the 1.86 Debye limit representing the dipole moment of an isolated molecule. This is a clear signature of the destabilization of the H-bond network, and the appearance of more and more water molecules with only weak interactions with their

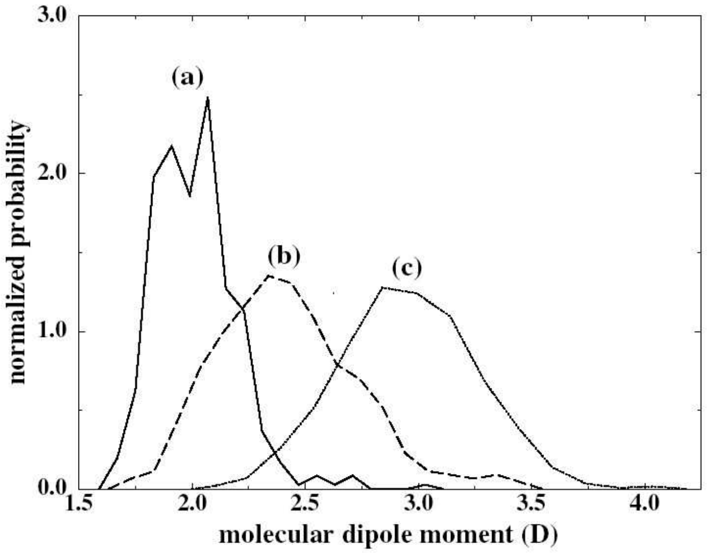

Figure 7: Distribution of the Wannier dipoles in supercritical water at a density of 0.32 g/cm^3 (a), and 0.73 g/cm^3 (b), compared with water at normal conditions (c).

neighbors (see Fig. 7).

It should be noted that the decomposition into Wannier dipoles is closer to the decomposition of the charge density into static (Szigeti) charges than to a decomposition into dynamical (Born) charges. The first one corresponds to a spatial decomposition of the total electronic charge density, while the second is connected with the force that appears on an atom in response to an applied electric field. Similarly, the Wannier dipoles provide a decomposition of the dielectric properties, maintaining the constraint that the total macroscopic polarization is correctly reproduced, but they do not describe the torque that would be exerted on the individual molecules by an electric field [42].

6.2 Open questions

There are several open questions that require further investigation, and represent intriguing directions towards a better formal understanding of the properties of the Wannier transformation.

We found that the MLWFs always turn out to be real in character, even if in the general case of a mesh of **k**-points different from Γ the Bloch orbitals themselves (and their periodic parts) will be complex. Even if this result seems plausible, we haven't been able to find or develop a proof for it (in the Γ-sampling formulation it becomes instead a trivial outcome, since the orbitals can always be chosen to be real to start with, propagating this characteristic across the minimization procedure).

Another related question has to do with the existence of concurrent minima for the localization functional in the space of the unitary matrices: we have found that in general there are multiple minima present (that's why we introduced a projection operation as a starting condition in (30)), but that only when at the physically-meaningful absolute minimum the Wannier functions turn out to be real, while in all other cases they are intrinsically complex. This characteristic alleviates the problems related to minimizing a multiple-minima functional, since the absolute minimum always displays this characteristic reality (also, we find that once the projection operation is introduced, minimization always proceeds to the right minimum, even with very poor or random initial choices). We attribute the failure in finding the global minimum in complex cases, if projections are not used, to the complex and random phase relationship that can take place between orbitals in the 3d topology of the Brillouin zone. In the Γ-sampling formulation, on the other hand, we never observe convergence into a local minimum, and the functional appears well-behaved, with a single basin of attraction leading to the global minimum.

Finally, the asymptotic behavior of localized Wannier functions for the general 3-dimensional case is still an open question. While des Cloizeaux [43, 44] proved exponential localization for the projection operator for a three-dimensional manifold, a similar result for the individual Wannier functions is still missing. In the case of one-dimensional systems, on the other hand, exponential localization has been proven [2]; this result has also been recently extended to the determination of the algebraic prefactors modulating the exponential decay [45].

7 Applications

Several papers have appeared in the recent literature that make significant use of the MLWFs. We highlight some of these in here, without the pretense of being exhaustive or of encompassing all published results. Broadly speaking, most applications can be grouped into one of three main themes:

- A tool to understand the nature of the chemical bond.
- A descriptor of local and global dielectric properties.
- A basis set for linear-scaling approaches and for constructing model Hamiltionians.

7.1 The Nature of the Chemical Bond

Once the electronic ground state has been decomposed into well-localized orbitals, it becomes possible and meaningful to study the spatial distribution and the average properties of their centers of charge (the WFCs). Silvestrelli et al. argued [29] that the WFCs can be a powerful tool to understand bonding in low-symmetry cases, representing both an insightful and an economical mapping of the continuous electronic degrees of freedom into a set of classical descriptors (the position of the WFCs, and the spread of their MLWFs). The benefits of this approach become apparent when studying the properties of disordered systems (see Fig. 8 for an example of the MLWFs in the distorted tetrahedral network of amorphous silicon). In amorphous solids the analysis of the microscopic properties is

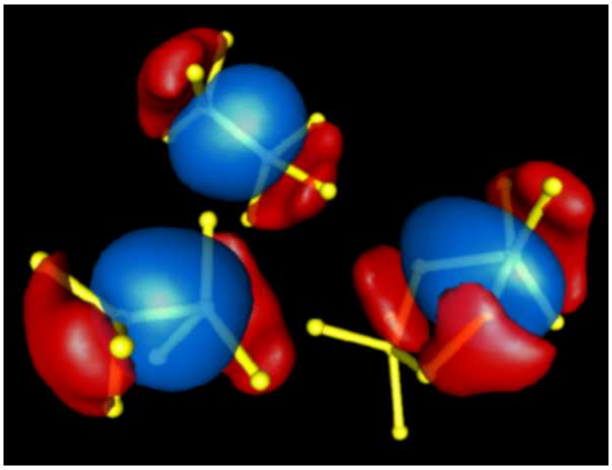

Figure 8: Maximally-localized Wannier functions in amorphous silicon, either around distorted but fourfold coordinated atoms, or in the presence of a fivefold defect. [From Ref. [46]]

usually based on the coordination number, i.e., on the number of atoms lying inside a sphere of a chosen radius r_c centered on the selected atom (r_c can be inferred with various degrees of confidence from the first minimum in the pair-correlation function). This purely geometrical analysis is completely blind to the actual electronic charge distribution, which ought to be important in any description of chemical bonding. An analysis of the full charge distribution and bonding in terms of the Wannier functions would be rather complex (albeit useful to characterize the most common defects [46]). Instead, just the knowledge of the positions of the WFCs and of their spreads can capture most of the chemistry in the system and can identify all the defects present. In this, the WFCs are treated as a second species of classical particles ("classical" electrons, represented by their centers), and the amorphous solid is treated as a statistical assembly of two kinds of particles, ions and WFCs.

We show in Fig. 9 the Si-Si $g(r)$ pair correlation function averaged over samples obtained with high-temperature first-principles molecular dynamics, and augment it with the plot of Si-WFC $g_w(r)$ pair correlation function. Both correlation functions display clear peaks (around $\simeq 2.4$ Åand $\simeq 1.2$ Å, respectively) and minima, showing that the electronic charge is mostly localized in the middle of the covalent bonds, as expected for amorphous silicon. Additional smaller peaks appear in the $g_w(r)$ correlation function for r around 0.5–1.0 Å (see inset); these peaks point to existence of a few anomalous MLWFs that are very close to a single Si atom. In order to make the analysis quantitative, we can calculate the usual coordination number (integrating the $g(r)$ up to its first minimum at $r_c = 2.80$ Å). We find that, on average, 96.5 % of the Si ions are fourfold coordinated, while 3.5 % are fivefold coordinated, in agreement with previous simulations [47]. We can now introduce our *novel bonding criterion*, based on the locations of the WFCs. The existence of a bond between two ions is defined by their sharing of a common WFC located within $r_w = 1.75$ Å of each ion (this is the position of the first minimum for the $g_w(r)$). Following this definition, we now find that 97.5 % of the Si ions are fourfold bonded; of the remaining

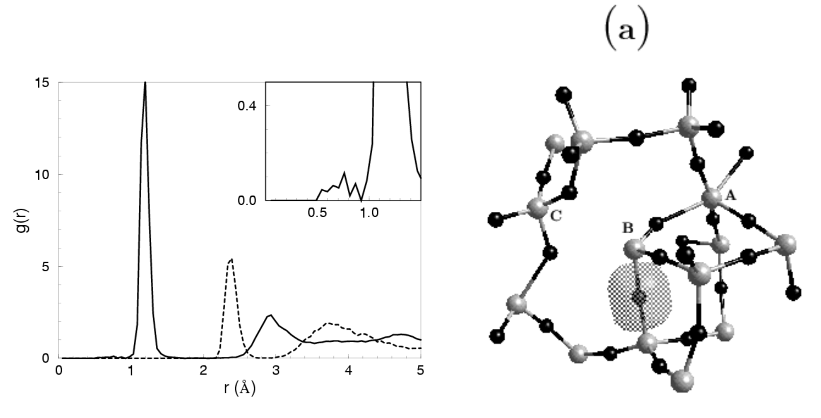

Figure 9: Left panel: Si-Si (dashed line) and Si-WFC (solid line) pair-correlation functions, from a 10 ps Car-Parrinello run on a 64-atom supercell. The detailed structure, in the range 0.0–1.5 Å, is shown in the inset. Right panel: Snapshots from 2 different timesteps in the simulation, corresponding to configurations where A and B maintain their coordination (5 and 4 respectively), but change their bonding (5→4 and 4→3 respectively). Small black "atoms" are the Wannier centers. [From Ref. [29]]

ions, only ∼ 0.6 % have five bonds, while the others are more or less equally divided into twofold-bonded and threefold-bonded ions. The total density of defective atoms that we obtain is similar to that of the coordination analysis, but now the electronic signature of the defects emerges in a remarkably different way.

This fact is best illustrated by inspection of some selected configurations from the molecular-dynamics runs. We show in the middle and right panels of Fig. 9 two different configurations that have the same coordination environment (e.g. for the case of ions A and B). For the initial configuration in (a) we obtain from our bonding analysis that ion A, fivefold coordinated, has also five bonds, while ion B, fourfold coordinated, has only three bonds (e.g. no WFC is found between ion B and ion C). As the ions move (see Fig. 9(b)). the electronic configuration also changes, and after about 10 ps the WFC located between ion A and ion B gets even closer to ion B, at a distance of 0.57 Å, and in such a way that the A–B bond is broken or at least severely weakened. In this configuration, according to our criterion, ion A is fourfold bonded, while ion B has only *two* bonds; further inspection of the density profile of one of these "lone pair" MLWFs shows how it is clearly different from a regular covalent bond. In addition, the spread is considerably larger, providing a very simple criteria that makes electronic defects straightforwardly identifiable in a MLWFs analysis.

Besides its application to the study of disordered networks [49, 50, 51], the above analysis can also be effectively employed to elucidate the chemical and electronic properties accompanying structural transformations. In a recent work on silicon nanoclusters under pressure [52, 53, 48], the location of the WFCs was monitored during compressive loading (up to 35 GPa) and unloading (see Fig. 10). The analysis of the "bond angles"

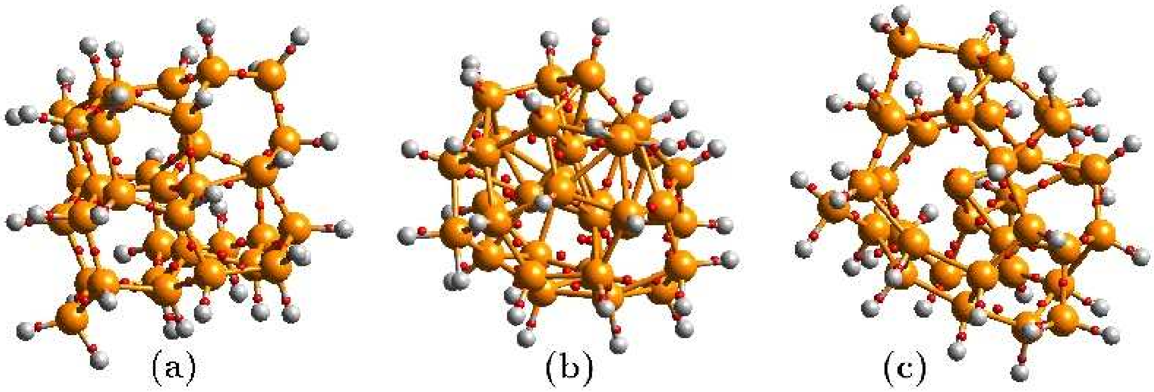

Figure 10: Collapse and amorphization of a Si cluster under pressure (increasing to 25 GPa (a), 35 GPa (b) and back to 5 GPa (c)). Small red "atoms" are the Wannier centers. [From Ref. [48]]

formed by two WFCs and their common silicon atom shows considerable departure from the tetrahedral rule at the transition pressure (Fig. 11). At the same pressure the ML-WFs become significantly more delocalized (inset of Fig. 11), hinting at a metallization transition similar to that happening for Si from the diamond structure into β-tin.

Interestingly, the MLWFs analysis can also point to structural defects that do not exhibit any significant electronic signature. Goedecker et al. [54] have recently predicted – entirely from first-principles – the existence of a new fourfold-coordinated defect that is stable inside the Si lattice (see Fig. 12). This defect had not been considered before, but displays by far the lowest formation energy – at the density-functional theory level – among all defects in silicon. Inspection of the relevant "defective" MLWFs reveals that their spreads remain actually very close to those typical of crystalline silicon, and that the WFCs remain equally shared between the atoms, in a very regular covalent arrangement. These considerations suggest that the electronic configuration is locally almost indistinguishable from that of the perfect lattice, making this defect difficult to detect with standard electronic probes. Also, a low activation energy is required for the self-annihilation of this defect; this consideration, in combination with the "stealth" electronic signature, hints at why such a defect could have eluded experimental discovery (if it does indeed exist !) despite the fact that Si is one of the best studied materials in the history of technology.

Moving towards more complex chemical systems, the MLWF analysis has been used in understanding and monitoring the nature of the bonding under varying thermodynamical conditions or along a chemical reaction in systems as diverse as ice [55], doped fullerenes [56], adsorbed organic molecules [57], ionic solids [58, 59] and in a study of the Ziegler-Natta polymerization [60]. This latter case (see Fig. 13) is a paradigmatic example of the chemical insight that can be gleaned following the WFCs in the course of an ab-initio simulation. In the Ziegler-Natta polymerization we have an interconversion of a double

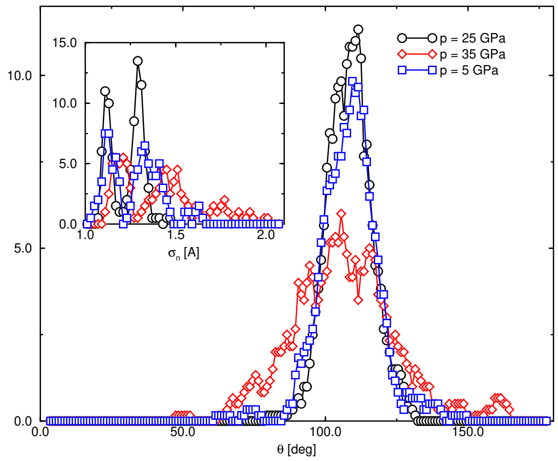

Figure 11: Distribution of the WFC-Si-WFC bond angles for the configurations shown in Fig. 10. The inset tracks in an histogram the spreads of the MLWFs at different pressures. [From Ref. [48]]

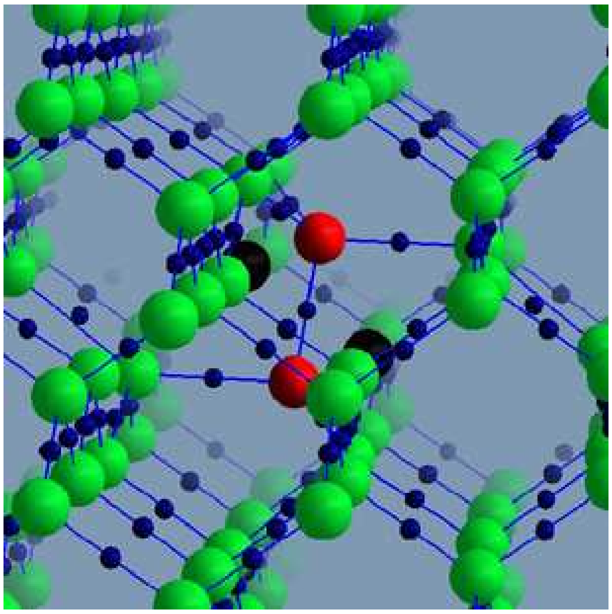

Figure 12: The recently-discovered fourfold coordinated defect in Si. Si atoms are in green, vacancies in black, and the centers of the MLWFs in blue, with a radius proportional to their spread. [From Ref. [54]]

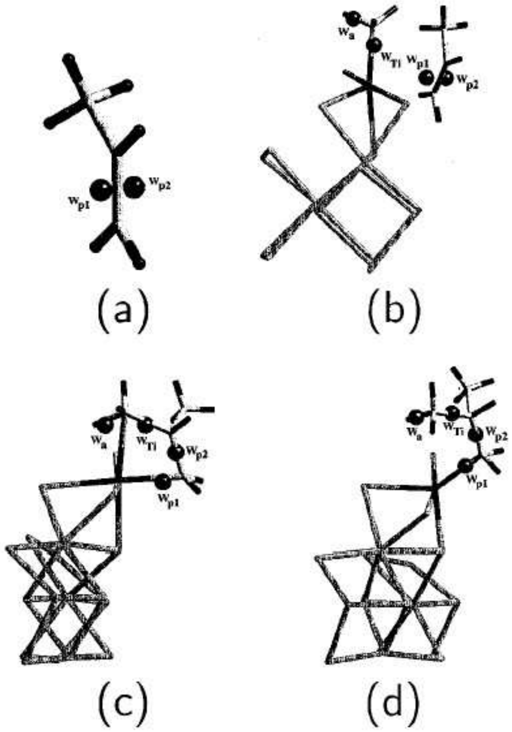

Figure 13: Propene polymerization at a Ti catalytic site on a $MgCl_2$ substrate. The evolution of the WFCs is shown, going from an isolated propene molecule (a) to the complexation with the catalyst (b) and to the formation of the polymeric chain (d) via the transition state (c). The breaking of the double carbon bond becomes clearly evident, as is the α-*agostic* interaction manifest in the displacement of one of the C-H centers in the methyl group. [From Ref. [60]]

carbon bond into a single bond, and a characteristic *agostic* interaction between the C-H bond and the activated metal center. Both become immediately visible once the WFCs are monitored, greatly aiding the interpretation of the complex chemical pathways.

As discussed before, the MLWF analysis has been pioneered by the group of M. Parrinello and applied initially to the study of the properties of liquid water. For example, we show in Fig. 14 (left panel) a snapshot from a molecular dynamics simulation, explicitly showing some of the dynamical connections along hydrogen bonds. The nature of the hydrogen bond becomes already explicit in the MLWFs for an isolated water dimer (center and right panels of Fig. 14), where the hybridization between orbitals in the two molecules is clearly visible. Applications of the Wannier-function technique to water have been numerous, from studies at normal conditions to high- and low-pressure phases at high temperature [39, 41, 40, 61, 62, 63]. Results from one of these simulations are shown in Fig. 15, during a fast dissociation events. The work on the structure of pure water has now been augmented by the study of the solvation and dielectric properties of ions in water [64, 65, 66, 67, 68]; recently even more complex biochemical systems have been investigated, ranging from wet DNA [69] to HIV-1 protease [70] or to phosphate groups in different environments (ATP, GTP and ribosomal units) [71, 72, 73, 74].

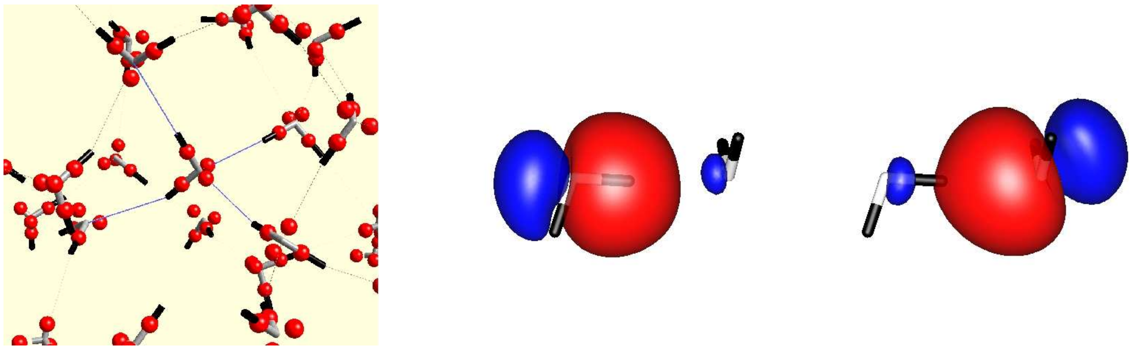

Figure 14: Left panel: WFCs (red) from a snapshot of a Car-Parrinello simulation of liquid water. The hydrogen atoms are in black and the oxygens in white; hydrogen bonds have also been highlighted. Center panel: MLWF for a O-H bond in a water dimer. Right panel: MLWF for a lone pair in a water dimer. [Left panel courtesy of P. L. Silvestrelli [41]]

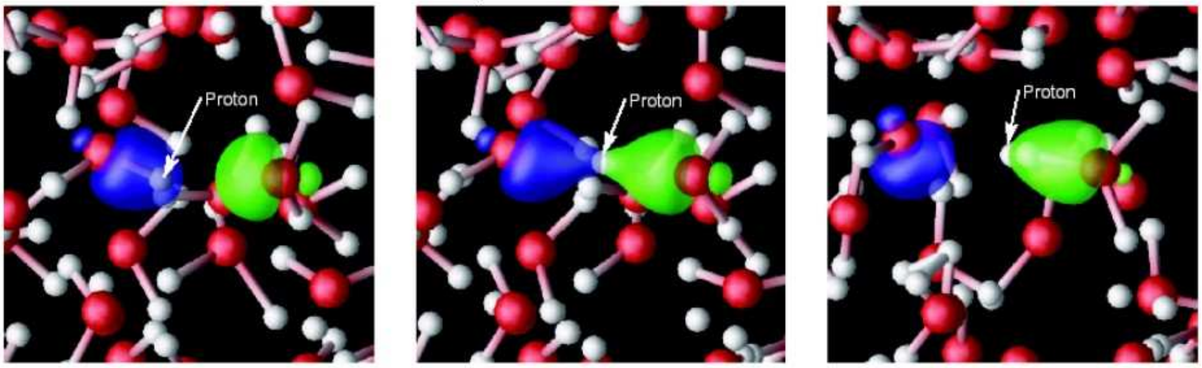

Figure 15: Snapshots of a rapid water-molecule dissociation under high-temperature (1390 K) and high-pressure (27 GPa) conditions; one of the MLWFs in the proton-donor molecule is highlighted in blue, and one of the MLWFs in the proton-acceptor molecule is highlighted in green. [From Ref. [62]]

Finally, localized orbitals can embody the chemical concept of transferable functional groups, and thus be used to construct a good approximation for the electronic-structure of complex systems starting for the orbitals for the different fragments [75].

7.2 Local and Global Dielectric Properties

The modern theory of polarization [8, 9] directly relates the vector sum of the centers of the Wannier functions to the polarization of an insulating system. This exact correspondence to a macroscopic observable (rigorously speaking, the change in polarization [76] upon a perturbation) cannot depend on the particular choice of representation: the sum of the Wannier centers is in fact invariant – as it should be – with respect to unitary transformations of the orbitals [35]. The existence of this exact relation between classical electrostatics and the quantum-mechanical WFCs suggests a heuristic identification by which the pattern of displacements of the WFCs can be regarded as defining a coarsegrained representation for the polarization field $\mathbf{P}(\mathbf{r})$. This identification is reinforced by the insightful chemical description of the ground-state electronic structure that single MLWFs provide, as shown in the previous section.

A natural application of this formalism is directed towards the description of the Born dynamical (effective) charges. The Born dynamical charges describe the change in macroscopic polarization induced by the displacement of a given ion. As such, they play a fundamental role in determining the lattice-dynamical properties of insulating crystals (e.g., the intensity of infrared absorption), and are a powerful tool to investigate the dielectric and ferroelectric properties of materials. They also determine the splitting of the infrared-active optical modes; in simpler compounds (e.g. GaAs) they can be determined from the experimental zone-center phonons. Using the MLWF representation, it becomes possible not only to calculate the Born charges Z^* from the vector displacements of the sum of the WFCs induced by an ionic displacement, but also to naturally decompose them into contributions originating from individual MLWFs. As an example, we have studied GaAs in a cubic supercell in which one Ga atom has been displaced along the [111] direction. From the resulting displacement of the Wannier centers we derive a value for Z^*_{Ga} of 2.04, in good agreement with other theoretical predictions. Moreover, in arriving at the total electronic $Z^{*,\mathrm{el}}_{\mathrm{Ga}}=-0.96$, we find contributions of -1.91, $+0.65$, and $+0.30$ from the groups of four first-neighbor, twelve second-neighbor, and remaining further-neighbor Wannier centers, respectively. It is interesting to note that inclusion of nearest-neighbor contributions alone would significantly overestimate the magnitude of $Z^{*,\mathrm{el}}_{\mathrm{Ga}}$, and that the second-neighbor Wannier centers move in the opposite direction to the Ga atom motion. If we repeat the calculation displacing one As atom, we obtain a total Z^*_{As} of -2.07. The electronic $Z^{*,\mathrm{el}}_{\mathrm{As}}=-7.07$ has now contributions of -1.74, -4.63, and -0.71 from the four first-neighbors, twelve second-neighbor, and remaining further-neighbor Wannier centers, respectively.

Such decomposition is particularly instructive in the case of perovskite ferroelectrics, which often display anomalously large effective charges in comparison to their nominal ionic value [77, 78]. The origin of this effect lies in the large dynamical charge transfer that takes place when moving away from the high-symmetry cubic phase (i.e., going from more ionic to more covalent bonding). Orbital hybridization is necessary for this transfer to take place and our localized-orbitals approach provides an insightful tool in describing these effects. If the bonding were purely ionic, electrons (and thus Wannier centers) would be firmly localized on each anion, and move rigidly with it. This is not the case in perovskites, and the anomalous contribution is linked to substantial hybridization between the oxygen p orbitals and the d orbitals of the atom in the octahedral cage (see Fig. 2 for a pictorial description of this phenomenon). The picture can be even more complex, with other group of bands playing a role in the anomalous dielectric behavior, where again the MLWFs decomposition can measure the different contributions from separate groups of bands (equivalently available in a Bloch picture [79, 80, 81]), but also from specific atoms or bonds inside a composite group of bands [19]).

Finally, Wannier functions are a particularly appropriate choice to study the effects of applied external fields on periodic or extended systems (periodic boundary conditions are in principle not compatible with constant applied fields). The localization properties of MLWFs have been directly exploited to calculate NMR chemical shifts [82]; also, even if not strictly necessary, MLWFs would allow for a straightforward implementation of recent proposals to describe the response to electric fields for periodic solids [83, 84].

7.3 MLWFs as a basis set: from linear-scaling to model Hamiltonians

One of the most attractive features calling for the use of localized orbitals in electronic-structure calculations is their ability to avoid computational bottlenecks deriving from non-local constraints. E.g., standard density-functional approaches suffer in the asymptotic limit from a cubic-scaling cost due to their orthonormality requirements. This factor of 8 can be easily identified by considering that if the size of a system studied is doubled, there will be twice as many orbitals to consider, each of them satisfying an orthonormality relation with twice as many orbitals, and with each overlap integrals having now a double cost (in order to keep the same resolution on a doubled integration domain). So, localization strategies are at the core of current efforts to develop truly linear-scaling approaches. For the case of orthonormality constraints, localized orbitals will only need to have those enforced with a small number of overlapping neighbors, and that number is generally independent of the system size.

A very promising implementation for a linear-scaling algorithm has been recently proposed in the context of (Diffusion) Quantum Monte Carlo calculations [10] and has already been applied to a variety of technologically-relevant nanoscale structures [85, 86]. In this formulation, the MLWFs representation is used to construct the Slater determinant for the trial wavefunction, at variance with the standard choice of single-electron eigenstates. The use of MLWFs makes the Slater determinant sparse, and with the additional benefits of introducing storage costs that are also linear-scaling. The benefits of this choice are immediately evident and shown in Fig. 16, with a plot for the cost of a single wavefunction evaluation as a function of the total number of electrons and for different choices for the basis set.

Besides this computational advantages, localized representations have long been used in theoretical condensed-matter theory to develop model Hamiltonians (e.g. Hubbard, t-J) able to capture the physics of strongly-correlated fermions. Some of these derivations are based on the Wannier picture, and recent works have taken the direct route of extracting the relevant interaction parameters from the MLWFs themselves [12, 13], with remarkable success in the description e.g. of the magnetic properties of cuprates. Similarly, MLWFs can be used to construct the Green's functions in the Landauer formulation of ballistic conductance [11], or to extend the formalism of correlated electrons to thermal transport properties [14].

Finally, less traditional approaches involve the construction of lattice Wannier functions

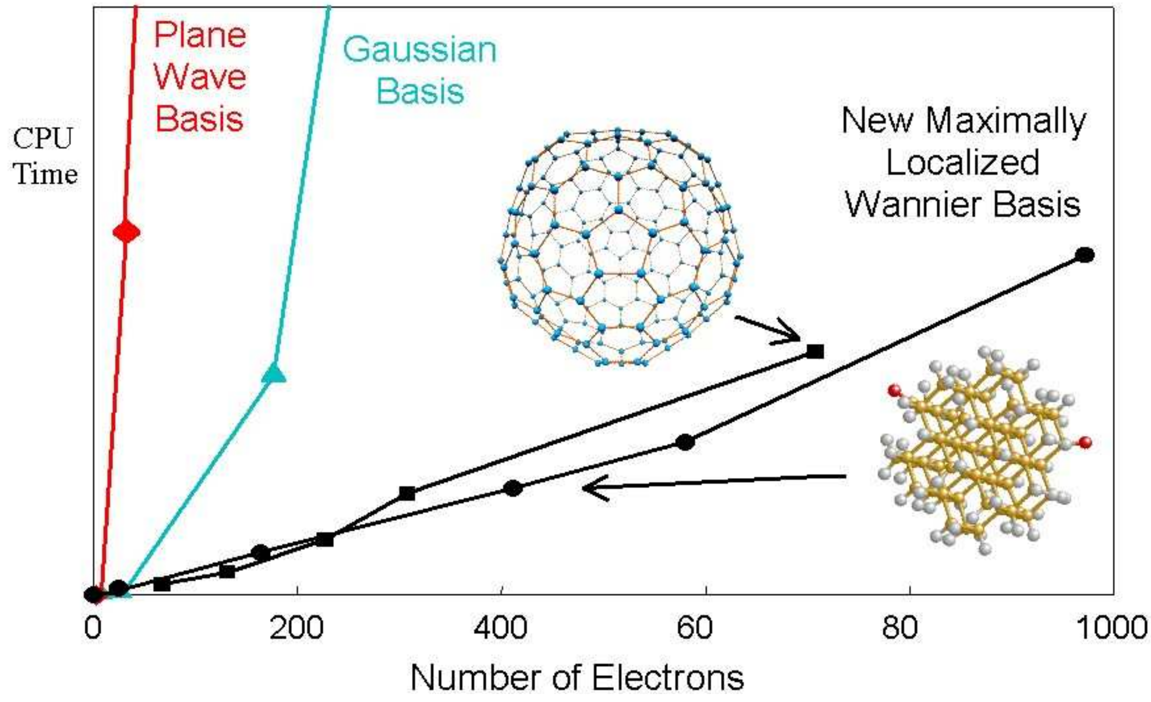

Figure 16: CPU time required to move a single configuration of electrons for one time step in silicon cluster and fullerenes, using a linear-scaling diffusion Monte Carlo approach that uses MLWFs as a basis set. [From Ref. [62]]

to model structural phase transitions in the solid-state [87, 88, 89], or, recently, photonic Wannier functions, with complete analogy between periodic electronic potentials and their Bloch or Wannier states, and periodic photonic lattices [90, 15, 16, 91].

7.4 Algorithmic Developments

We conclude by mentioning a number of algorithms and theoretical developments closely linked to the formulation presented in this work. These range from the extension of the MLWFs representation to the all-electron case [59], to the development of alternative minimization and localization algorithms [31, 28, 24, 92, 27], and to the many-body formulation of the position and localization operators [93, 94, 95, 96, 97].

8 Conclusions

We have described a theoretical and algorithmic framework for transforming the Bloch eigenfunctions into a localized Wannier representation. For a composite group of bands that is isolated (i.e., separated by gaps from other groups), optimal localization properties are obtained by minimizing a well-defined localization functional corresponding to the sum of the second moments of the orbitals around their centers of charge. The localization algorithm proceeds by iterating the degrees of freedom of the Wannier transformation, i.e., a continuous set of unitary matrices defined everywhere in the Brillouin zone, with dimension equal to the number of bands to be transformed. This criterion is the extension to the solid state of the Boys localization criterion for isolated molecules, and reduces to it when dealing with large supercells containing isolated systems. The procedure has been extended to deal with entangled energy bands, i.e., to the case when the bands of interests are not separated by gaps from other bands. In this case, localization becomes a two-fold process. First we extract a maximally-connected subspace of chosen dimension from a given energy window, essentially requiring that the extracted manifold had minimal dispersion of its projection operator across the Brillouin zone. Second, we extract the maximally-localized Wannier functions from this well-connected subspace using our standard localization procedure. Lastly, we have shown how the localization algorithm simplifies considerably in the special case of Γ-point Brillouin-zone sampling appropriate for large supercells, and outlined the extension to the use of ultrasoft pseudopotentials for this case.

Applications of our approach are already numerous, and we have presented some of the early results available in the literature. Broadly speaking, there are three classes of applications where MLWFs have found natural use.

- The method is useful for the description of the chemical properties of complex systems, thanks to the intuitive connection between the MLWFs and the shape and symmetry of individual bonds, and the ability of MLWFs to summarize information about the electronic states in terms of their centers of charge.
- The dielectric properties of complex materials is well described in a local language. In particular, the macroscopic polarization is exactly related to the vector sum of the valence-band Wannier centers via the modern theory of polarization. Thus, local polarization properties can be heuristically represented by a field of Wannier dipoles, and thus, to the specific activity of well-defined atom- or bond-like MLWFs.
- MLWFs provide an efficient and accurate minimal basis set suitable for applications ranging from linear-scaling approaches, to the development of model Hamiltonians for strongly-correlated systems or for the electronic-transport properties, to applications outside the traditional realm of electronic-structure calculations (e.g., in the determination of lattice Wannier functions or photonic Wannier functions).

Further applications of this approach are envisioned, thanks to the ever-increasing availability of public electronic-structure software under the broad umbrella of the GNU Project / Free Software Foundation (see below), and its current incorporation in widely-used or distributed electronic-structure packages, such as the Car-Parrinello molecular-dynamics codes CPMD (IBM/MPI Stuttgart), JEEP (LLNL), and CP90 (Princeton University/EPFL Lausanne/University of Pisa/MIT).

9 Acknowledgments

This work was supported by NSF grants DMR-96-13648, DMR-9981193, and DMR-0233925, and by a NSF-CISE Postdoctoral Fellowship ASC-96-25885. We would like to thank W. Kohn, Q. Niu, and R. Resta for many illuminating discussions, and M. Boero, M. Fornari, G. Galli, S. Goedecker, R. Martonak, C. Molteni, M. Parrinello, P. Silvestrelli, and A. J. Williamson for granting us permission to use figures from their work in this review.

10 Web site: www.wannier.org

The maximally-localized Wannier code for isolated, composite groups of bands is available under the GNU Public License at www.wannier.org, and can be interfaced to any electronic structure code able to calculate the scalar products $M_{mn}^{(\mathbf{k},\mathbf{b})} = \langle u_{m\mathbf{k}}|u_{n,\mathbf{k}+\mathbf{b}}\rangle$. A public-domain version that includes the disentanglement procedure is also in progress.

Appendix: Extension to ultrasoft pseudopotentials

The extension of the localization formalism to the case of ultrasoft pseudopotentials *for the case of* Γ*-sampling only* is fairly straightforward and has been recently implemented (see Refs. [98, 99]). The formalism of Sec. 4.2 can be followed, where the appropriate scalar products M_{ij}^l introduced in (39) are now calculated via the augmentation operator $K(\mathbf{r})$, as defined in Ref. [100, 101]:

$$\begin{aligned} M_{mn}^l &= \langle w_m|K(\mathbf{r})e^{-i\mathbf{G}_l\cdot\mathbf{r}}|w_n\rangle \\ &= \langle w_m(\mathbf{r})|e^{-i\mathbf{G}_l\cdot\mathbf{r}}|w_n(\mathbf{r})\rangle + \sum_{ij,I}\int Q_{ij}^I(\mathbf{r})e^{-i\mathbf{G}_l\cdot\mathbf{r}}d\mathbf{r}\ \langle w_m|\beta_i^I\rangle\langle\beta_j^I|w_n\rangle\ . \end{aligned} \tag{48}$$

We foresee no particular difficulty in extending the ultrasoft MLWFs formalism to the case of general Monkhorst-Pack meshes, but we are not aware of any actual implementation to date.

References

[1] G. H. Wannier, "The structure of electronic excitation levels in insulating crystals," *Physical Review*, vol. 52, p. 191, 1937.

[2] W. Kohn, "Analytic properties of Bloch waves and Wannier functions," *Physical Review*, vol. 115, pp. 809–821, 1959.

[3] J. des Cloizeaux, "Orthogonal orbitals and generalized Wannier functions," *Physical Review*, vol. 129, no. 2, p. 554, 1963.

[4] S. F. Boys, “Construction of molecular orbitals to be approximately invariant for changes from one molecule to another,” *Reviews of Modern Physics*, vol. 32, p. 296, 1960.

[5] J. M. Foster and S. F. Boys, “Canonical configurational interaction procedure,” *Reviews of Modern Physics*, vol. 32, pp. 300–302, 1960.

[6] J. M. Foster and S. F. Boys, “A quantum variational calculation for HCHO,” *Reviews of Modern Physics*, vol. 32, pp. 303–304, 1960.

[7] S. F. Boys, “Localized orbitals and localized adjustment functions,” in *Quantum Theory of Atoms, Molecules, and the Solid State* (P.-O. Löwdin, ed.), pp. 253–262, New York: Academic Press, 1966.

[8] R. D. King-Smith and D. Vanderbilt, “Theory of polarization of crystalline solids,” *Physical Review B*, vol. 47, no. 3, pp. 1651–1654, 1993.

[9] R. Resta, “Macroscopic polarization in crystalline dielectrics - the geometric phase approach,” *Reviews of Modern Physics*, vol. 66, no. 3, pp. 899–915, 1994.

[10] A. J. Williamson, R. Q. Hood, and J. C. Grossman, “Linear-scaling quantum Monte Carlo calculations,” *Physical Review Letters*, vol. 87, no. 24, p. 246406, 2001.

[11] A. Calzolari, N. Marzari, I. Souza, and M. Buongiorno Nardelli, “Ab-initio transport properties of nanostructures from maximally-localized Wannier functions,” *in preparation*, 2003.

[12] W. Ku, H. Rosner, W. E. Pickett, and R. T. Scalettar, “Insulating ferromagnetism in La4Ba2Cu2O10: An ab initio Wannier function analysis,” *Physical Review Letters*, vol. 89, no. 16, p. 167204, 2002.

[13] I. Schnell, G. Czycholl, and R. C. Albers, “Hubbard-U calculations for Cu from first-principle Wannier functions,” *Physical Review B*, vol. 65, no. 7, p. 075103, 2002.

[14] I. Paul and G. Kotliar, “Thermal transport for many-body tight-binding models,” *Physical Review B*, vol. 67, no. 11, p. 115131, 2003.

[15] D. M. Whittaker and M. P. Croucher, “Maximally localized Wannier functions for photonic lattices,” *Physical Review B*, vol. 67, no. 8, p. 085204, 2003.

[16] A. Garcia-Martin, D. Hermann, F. Hagmann, K. Busch, and P. Wolfle, “Defect computations in photonic crystals: a solid state theoretical approach,” *Nanotechnology*, vol. 14, no. 2, pp. 177–183, 2003.

[17] N. Marzari and D. Vanderbilt, “Maximally localized generalized Wannier functions for composite energy bands,” *Physical Review B*, vol. 56, no. 20, pp. 12847–12865, 1997.

[18] E. I. Blount, "Formalisms of band theory," in *Solid State Physics* (F. Seitz and D. Turnbull, eds.), vol. 13, pp. 305–373, New York: Academic Press, 1962.

[19] N. Marzari and D. Vanderbilt, "Maximally-localized Wannier functions in perovskites: Cubic $BaTiO_3$," in *First-principles calculations for ferroelectrics* (R. E. Cohen, ed.), vol. 436, pp. 146–155, Woodbury NY: AIP Conference Proceedings, 1998.

[20] B. Sporkmann and H. Bross, "Calculation of Wannier functions for Fcc transition-metals by Fourier transformation of Bloch functions," *Physical Review B*, vol. 49, no. 16, pp. 10869–10876, 1994.

[21] B. Sporkmann and H. Bross, "Calculation of Wannier functions for zinc-blende-type semiconductors," *Journal of Physics-Condensed Matter*, vol. 9, no. 26, pp. 5593–5608, 1997.

[22] S. Satpathy and Z. Pawlowska, "Construction of bond-centered Wannier functions for silicon valence bands," *Physica Status Solidi B-Basic Research*, vol. 145, no. 2, pp. 555–565, 1988.

[23] U. Stephan, D. A. Drabold, and R. M. Martin, "Improved accuracy and acceleration of variational order-N electronic-structure computations by projection techniques," *Physical Review B*, vol. 58, no. 20, pp. 13472–13481, 1998.

[24] C. Sgiarovello, M. Peressi, and R. Resta, "Electron localization in the insulating state: Application to crystalline semiconductors," *Physical Review B*, vol. 64, no. 11, p. 115202, 2001.

[25] B. N. Flury and W. Gautschi, "An algorithm for the simultaneous orthogonal transformation of several positive definite symmetric matrices to nearly orthogonal form," *SIAM Journal on Scientific and Statistical Computing*, vol. 7, no. 1, pp. 169–184, 1986.

[26] J.-F. Cardoso and A. Souloumiac, "Jacobi angles for simultaneous diagonalization," *SIAM Journal on Matrix Analysis and Applications*, vol. 17, no. 1, pp. 161–164, 1996.

[27] F. Gygi, J.-L. Fattebert, and E. Schwegler, "Computation of maximally localized Wannier functions using a simultaneous diagonalization algorithm," *preprint*, vol. RL-JC-151591, pp. 1–12, 2003.

[28] G. Berghold, C. J. Mundy, A. H. Romero, J. Hutter, and M. Parrinello, "General and efficient algorithms for obtaining maximally localized Wannier functions," *Physical Review B*, vol. 61, no. 15, pp. 10040–10048, 2000.

[29] P. L. Silvestrelli, N. Marzari, D. Vanderbilt, and M. Parrinello, "Maximally-localized Wannier functions for disordered systems: Application to amorphous silicon," *Solid State Communications*, vol. 107, no. 1, pp. 7–11, 1998.

[30] A. Selloni, P. Carnevali, R. Car, and M. Parrinello, "Localization, hopping, and diffusion of electrons in molten- salts," *Physical Review Letters*, vol. 59, no. 7, pp. 823–826, 1987.

[31] P. L. Silvestrelli, "Maximally localized Wannier functions for simulations with supercells of general symmetry," *Physical Review B*, vol. 59, no. 15, pp. 9703–9706, 1999.

[32] I. Souza, N. Marzari, and D. Vanderbilt, "Maximally localized Wannier functions for entangled energy bands," *Physical Review B*, vol. 65, no. 3, p. 035109, 2002.

[33] C. Edmiston and K. Ruedenberg, "Localized atomic and molecular orbitals," *Reviews of Modern Physics*, vol. 35, pp. 457–465, 1963.

[34] J. Pipek and P. G. Mezey, "A fast intrinsic localization procedure applicable for ab-initio and semiempirical linear combination of atomic orbital wave-functions," *Journal of Chemical Physics*, vol. 90, no. 9, pp. 4916–4926, 1989.

[35] D. Vanderbilt and R. D. King-Smith, "Electric polarization as a bulk quantity and its relation to surface-charge," *Physical Review B*, vol. 48, no. 7, pp. 4442–4455, 1993.

[36] J. P. Foster and F. Weinhold, "Natural hybrid orbitals," *Journal of the American Chemical Society*, vol. 102, pp. 7211–7218, 1980.

[37] I. Souza, R. M. Martin, N. Marzari, X. Y. Zhao, and D. Vanderbilt, "Wannier-function description of the electronic polarization and infrared absorption of high-pressure hydrogen," *Physical Review B*, vol. 62, no. 23, pp. 15505–15520, 2000.

[38] P. Fernandez, A. DalCorso, A. Baldereschi, and F. Mauri, "First-principles Wannier functions of silicon and gallium arsenide," *Physical Review B*, vol. 55, no. 4, pp. R1909–R1913, 1997.

[39] P. L. Silvestrelli and M. Parrinello, "Water molecule dipole in the gas and in the liquid phase," *Physical Review Letters*, vol. 82, no. 16, pp. 3308–3311, 1999.

[40] M. Boero, K. Terakura, T. Ikeshoji, C. C. Liew, and M. Parrinello, "Hydrogen bonding and dipole moment of water at supercritical conditions: A first-principles molecular dynamics study," *Physical Review Letters*, vol. 85, no. 15, pp. 3245–3248, 2000.

[41] P. L. Silvestrelli and M. Parrinello, "Structural, electronic, and bonding properties of liquid water from first principles," *Journal of Chemical Physics*, vol. 111, no. 8, pp. 3572–3580, 1999.

[42] A. Pasquarello and R. Resta, "Dynamical monopoles and dipoles in a condensed molecular system: The case of liquid water," *in preparation*, 2003.

[43] J. D. des Cloizeaux, "Energy bands and projection operators in a crystal: Analytic and asymptotic properties," *Physical Review*, vol. 135, pp. A685–A697, 1964.

[44] J. D. des Cloizeaux, "Analytical properties of n-dimensional energy bands and Wannier functions," *Physical Review*, vol. 135, pp. A698–A707, 1964.

[45] L. X. He and D. Vanderbilt, "Exponential decay properties of Wannier functions and related quantities," *Physical Review Letters*, vol. 86, no. 23, pp. 5341–5344, 2001.

[46] M. Fornari, N. Marzari, M. Peressi, and A. Baldereschi, "Wannier functions characterization of floating bonds in a-Si," *Computational Materials Science*, vol. 20, no. 3-4, pp. 337–342, 2001.

[47] I. Stich, R. Car, and M. Parrinello, "Amorphous-silicon studied by ab-initio molecular-dynamics - preparation, structure, and properties," *Physical Review B*, vol. 44, no. 20, pp. 11092–11104, 1991.

[48] R. Martonak, C. Molteni, and M. Parrinello, "A new constant-pressure ab initio/classical molecular dynamics method: simulation of pressure-induced amorphization in a Si35H36 cluster," *Computational Materials Science*, vol. 20, no. 3-4, pp. 293–299, 2001.

[49] V. Meregalli and M. Parrinello, "An anomalous alloy: YxSi1-x," *Solid State Communications*, vol. 117, no. 7, pp. 441–444, 2001.

[50] S. H. N. Lim, D. G. McCullooch, A. R. Merchant, N. A. Marks, M. M. M. Bilek, and D. R. McKenzie, "Wannier function analysis for understanding disordered structures generated using Car-Parrinello molecular dynamics," *Molecular Simulation*, vol. 28, no. 10-11, pp. 971–979, 2002.

[51] P. Fitzhenry, M. M. M. Bilek, N. A. Marks, N. C. Cooper, and D. R. McKenzie, "Wannier function analysis of silicon-carbon alloys," *Journal of Physics-Condensed Matter*, vol. 15, no. 2, pp. 165–173, 2003.

[52] R. Martonak, C. Molteni, and M. Parrinello, "Ab initio molecular dynamics with a classical pressure reservoir: Simulation of pressure-induced amorphization in a Si35H36 cluster," *Physical Review Letters*, vol. 84, no. 4, pp. 682–685, 2000.

[53] C. Molteni, R. Martonak, and M. Parrinello, "First principles molecular dynamics simulations of pressure- induced structural transformations in silicon clusters," *Journal of Chemical Physics*, vol. 114, no. 12, pp. 5358–5365, 2001.

[54] S. Goedecker, T. Deutsch, and L. Billard, "A fourfold coordinated point defect in silicon," *Physical Review Letters*, vol. 88, no. 23, p. 235501, 2002.

[55] M. Bernasconi, P. L. Silvestrelli, and M. Parrinello, "Ab initio infrared absorption study of the hydrogen-bond symmetrization in ice," *Physical Review Letters*, vol. 81, no. 6, pp. 1235–1238, 1998.

[56] I. M. L. Billas, C. Massobrio, M. Boero, M. Parrinello, W. Branz, F. Tast, N. Malinowski, M. Heinebrodt, and T. P. Martin, "First principles calculations of Si doped fullerenes: Structural and electronic localization properties in C59Si and C58Si2," *Journal of Chemical Physics*, vol. 111, no. 15, pp. 6787–6796, 1999.

[57] P. L. Silvestrelli, F. Ancilotto, and F. Toigo, "Adsorption of benzene on Si(100) from first principles," *Physical Review B*, vol. 62, no. 3, pp. 1596–1599, 2000.

[58] L. Bernasconi, P. A. Madden, and M. Wilson, "Ionic to molecular transition in AlCl3: an examination of the electronic structure," *Physchemcomm*, vol. 5, no. 1, pp. 1–11, 2002.

[59] M. Posternak, A. Baldereschi, S. Massidda, and N. Marzari, "Maximally localized wannier functions in antiferromagnetic MnO within the FLAPW formalism," *Physical Review B*, vol. 65, no. 18, p. 184422, 2002.

[60] M. Boero, M. Parrinello, S. Huffer, and H. Weiss, "First-principles study of propene polymerization in Ziegler-Natta heterogeneous catalysis," *Journal of the American Chemical Society*, vol. 122, no. 3, pp. 501–509, 2000.

[61] M. Boero, K. Terakura, T. Ikeshoji, C. C. Liew, and M. Parrinello, "Water at supercritical conditions: A first principles study," *Journal of Chemical Physics*, vol. 115, no. 5, pp. 2219–2227, 2001.

[62] E. Schwegler, G. Galli, F. Gygi, and R. Q. Hood, "Dissociation of water under pressure," *Physical Review Letters*, vol. 87, no. 26, p. 265501, 2001.

[63] A. H. Romero, P. L. Silvestrelli, and M. Parrinello, "Compton scattering and the character of the hydrogen bond in ice I-h," *Journal of Chemical Physics*, vol. 115, no. 1, pp. 115–123, 2001.

[64] F. C. Lightstone, E. Schwegler, R. Q. Hood, F. Gygi, and G. Galli, "A first principles molecular dynamics simulation of the hydrated magnesium ion," *Chemical Physics Letters*, vol. 343, no. 5-6, pp. 549–555, 2001.

[65] E. Schwegler, G. Galli, and F. Gygi, "Conformational dynamics of the dimethyl phosphate anion in solution," *Chemical Physics Letters*, vol. 342, no. 3-4, pp. 434–440, 2001.

[66] D. J. Tobias, P. Jungwirth, and M. Parrinello, "Surface solvation of halogen anions in water clusters: An ab initio molecular dynamics study of the Cl-(H2O)(6) complex," *Journal of Chemical Physics*, vol. 114, no. 16, pp. 7036–7044, 2001.

[67] S. Raugei and M. L. Klein, "An ab initio study of water molecules in the bromide ion solvation shell," *Journal of Chemical Physics*, vol. 116, no. 1, pp. 196–202, 2002.

[68] I. Bako, J. Hutter, and G. Palinkas, "Car-parrinello molecular dynamics simulation of the hydrated calcium ion," *Journal of Chemical Physics*, vol. 117, no. 21, pp. 9838–9843, 2002.

[69] F. L. Gervasio, P. Carloni, and M. Parrinello, "Electronic structure of wet DNA," *Physical Review Letters*, vol. 89, no. 10, p. 108102, 2002.

[70] S. Piana, D. Sebastiani, P. Carloni, and M. Parrinello, "Ab initio molecular dynamics-based assignment of the protonation state of pepstatin A/HIV-1 protease cleavage site," *Journal of the American Chemical Society*, vol. 123, no. 36, pp. 8730–8737, 2001.

[71] F. Alber, G. Folkers, and P. Carloni, "Dimethyl phosphate: Stereoelectronic versus environmental effects," *Journal of Physical Chemistry B*, vol. 103, no. 29, pp. 6121–6126, 1999.

[72] T. J. Minehardt, N. Marzari, R. Cooke, E. Pate, P. A. Kollman, and R. Car, "A classical and ab-initio study of the interaction of the myosin triphosphate binding domain with ATP," *Biophysical Journal*, vol. 82, no. 2, pp. 660–675, 2002.

[73] A. Cavalli and P. Carloni, "Enzymatic GTP hydrolysis: Insights from an ab initio molecular dynamics study," *Journal of the American Chemical Society*, vol. 124, no. 14, pp. 3763–3768, 2002.

[74] K. Spiegel and P. Carloni, "Electrostatic role of phosphate 2485 in the large ribosomal unit from H-marismortui," *Journal of Physical Chemistry B*, vol. 107, no. 9, pp. 2091–2097, 2003.

[75] D. M. Benoit, D. Sebastiani, and M. Parrinello, "Accurate total energies without self-consistency," *Physical Review Letters*, vol. 87, no. 22, p. 226401, 2001.

[76] R. Resta, "Theory of the electric polarization in crystals," *Ferroelectrics*, vol. 136, no. 1-4, pp. 51–55, 1992.

[77] W. Zhong, R. D. King-Smith, and D. Vanderbilt, "Giant lo-to splitting in perovskite ferroelectrics," *Physical Review Letters*, vol. 72, no. 22, pp. 3618–3621, 1994.

[78] P. Ghosez, J. P. Michenaud, and X. Gonze, "Dynamical atomic charges: The case of ABO(3) compounds," *Physical Review B*, vol. 58, no. 10, pp. 6224–6240, 1998.

[79] P. Ghosez and X. Gonze, "Band-by-band decompositions of the Born effective charges," *Journal of Physics-Condensed Matter*, vol. 12, no. 43, pp. 9179–9188, 2000.

[80] M. Veithen, X. Gonze, and P. Ghosez, "Electron localization: Band-by-band decomposition and application to oxides," *Physical Review B*, vol. 66, no. 23, p. 235113, 2002.

[81] U. V. Waghmare, N. A. Spaldin, H. C. Kandpal, and R. Seshadri, "First-principles indicators of metallicity and cation off- centricity in the IV-VI rocksalt chalcogenides of divalent Ge, Sn, and Pb," *Physical Review B*, vol. 67, no. 12, p. 125111, 2003.

[82] D. Sebastiani and M. Parrinello, "A new ab-initio approach for NMR chemical shifts in periodic systems," *Journal of Physical Chemistry A*, vol. 105, no. 10, pp. 1951–1958, 2001.

[83] I. Souza, J. Íñiguez, and D. Vanderbilt, "First-principles approach to insulators in finite electric fields," *Physical Review Letters*, vol. 89, no. 11, p. 117602, 2002.

[84] P. Umari and A. Pasquarello, "Ab initio molecular dynamics in a finite homogeneous electric field," *Physical Review Letters*, vol. 89, no. 15, p. 157602, 2002.

[85] A. J. Williamson, J. C. Grossman, R. Q. Hood, A. Puzder, and G. Galli, "Quantum Monte Carlo calculations of nanostructure optical gaps: Application to silicon quantum dots," *Physical Review Letters*, vol. 89, no. 19, p. 196803, 2002.

[86] A. Puzder, A. J. Williamson, J. C. Grossman, and G. Galli, "Surface control of optical properties in silicon nanoclusters," *Journal of Chemical Physics*, vol. 117, no. 14, pp. 6721–6729, 2002.

[87] K. M. Rabe and U. V. Waghmare, "Localized basis for effective lattice hamiltonians: Lattice Wannier functions," *Physical Review B*, vol. 52, no. 18, pp. 13236–13246, 1995.

[88] J. Íñiguez, A. Garcia, and J. M. Pérez-Mato, "Optimized local modes for lattice-dynamical applications," *Physical Review B*, vol. 61, no. 5, pp. 3127–3130, 2000.

[89] R. Caracas, K. M. Rabe, and X. Gonze, "Automatic generation of lattice Wannier functions," *in preparation*, 2003.

[90] I. Talanina and C. M. de Sterke, "Bloch waves and Wannier functions in periodic superstructure Bragg gratings," *Physical Review A*, vol. 62, no. 4, p. 043802, 2000.

[91] E. A. Ostrovskaya and Y. S. Kivshar, "Matter-wave gap solitons in atomic band-gap structures," *Physical Review Letters*, vol. 90, no. 16, p. 160407, 2003.

[92] M. Iannuzzi and M. Parrinello, "Wave-function localization in reciprocal space," *Physical Review B*, vol. 66, no. 15, p. 155209, 2002.

[93] R. Resta, "Quantum-mechanical position operator in extended systems," *Physical Review Letters*, vol. 80, no. 9, pp. 1800–1803, 1998.

[94] R. Resta and S. Sorella, "Electron localization in the insulating state," *Physical Review Letters*, vol. 82, no. 2, pp. 370–373, 1999.

[95] J. Zak, "Comment on "quantum-mechanical position operator in extended systems"," *Physical Review Letters*, vol. 85, no. 5, pp. 1138–1138, 2000.

[96] I. Souza, T. Wilkens, and R. M. Martin, "Polarization and localization in insulators: Generating function approach," *Physical Review B*, vol. 62, no. 3, pp. 1666–1683, 2000.

[97] E. Koch and S. Goedecker, "Locality properties and Wannier functions for interacting systems," *Solid State Communications*, vol. 119, no. 2, pp. 105–109, 2001.

[98] L. Bernasconi and P. A. Madden, "Optimally localized Wannier functions within the Vanderbilt ultrasoft pseudo-potential formalism," *Journal of Molecular Structure-Theochem*, vol. 544, pp. 49–60, 2001.

[99] Y. Wu, M. Manu, P. Giannozzi, N. Marzari, and R. Car, "Implementation of the maximally-localized Wannier functions in an ultrasoft Car-Parrinello molecular dynamics code," in *CP90 code*, Princeton University, 2001.

[100] D. Vanderbilt, "Soft self-consistent pseudopotentials in a generalized eigenvalue formalism," *Physical Review B*, vol. 41, no. 11, pp. 7892–7895, 1990.

[101] K. Laasonen, R. Car, C. Lee, and D. Vanderbilt, "Implementation of ultrasoft pseudopotentials in ab-initio molecular-dynamics," *Physical Review B*, vol. 43, no. 8, pp. 6796–6799, 1991.